HIGH ENERGY LASER WINDOWS

R. W. Rice

Naval Research Laboratory

Prepared for:

Advanced Research Projects Agency

31 December 1974

High Energy Laser Windows

Semi-Annual Report No. 5
For period ending 31 December 1974

Sponsored by
Advanced Research Projects Agency
ARPA Order 2031

NAVAL RESEARCH LABORATORY
Washington, D.C. 20375

Related Rept - AD 784991

ARPA Order
2031

Program Code
3D10

Principal Investigator:
R. W. Rice
(202)767-2131

Contractor:
U. S. Naval Research Laboratory

Effective Date of Contract:
1 July 1974

Contract Expiration Date:
30 June 1975

Amount of Contract:
$225K

FOREWORD

This semi-annual technical report summarizes work performed by personnel of the U. S. Naval Research Laboratory, Washington, D. C. 20375, under ARPA Order 2031. The program was coordinated by Mr. R. W. Rice and Dr. P. F. Becher of NRL, and monitored by Dr. C. M. Stickley of ARPA. The report covers the period 1 July 1974 through 31 December 1974. The list of publications and presentations at the beginning of the report illustrate several of the major results of this program. Some material contained in the report from Navy supported programs is included since it should be of general interest to those concerned with laser windows.

PUBLICATIONS AND PRESENTATIONS

1. Presented at and to be published in the Proceedings of the 4th Conference on Laser Window Materials, Tucson, Arizona, Nov. 1974.

   a. Stierwalt, D.L. and Hass, M., Elimination of Surface Absorption in KCl.

   b. Boyer, L., Harrington, J.A., Hass, M. and Rosenstock, H., Multiphonon Absorption in Laser Window Materials.

   c. Hass, M., Davisson, J.W. and Babiskin, J., Improved Laser Calorimetric Techniques.

   d. Klein, P.H., and Davisson, J.W., Growth, Surface Finishing and Optical Characterization of Sodium Fluoride and Other Fluoride Laser Window Crystals.

   e. Becher, P.F., Freiman, S.W., Rice, R.W., Klein, P.H. and Krulfeld, M., Fracture Behavior and Residual Forging Strain Effects in Strengthening KCl.

   f. Rice, R.W., Freiman, S.W., Mecholsky, J.J., and Wurst, J.C., Fracture of ZnSe and As_2S_3 Laser Window Materials.

   g. Becher, P.F., Mecholsky, J.J., Spann, J.R., and Rice, R.W., Laser Testing of Uncoated KCl.

2. Boyer, L., Harrington, J.A., Hass, M. and Rosenstock, H., Multiphonon Absorption in Ionic Crystals, to be published in Phys. Rev., Mar. 1975.

3. Hass, M., Davisson, J.W., Rosenstock, H. and Babiskin, J., Measurement of Very Low Absorption Coefficients by Laser Calorimetry, Accepted for Publication in Appl. Optics.

4. Klein, P.H., Krufeld, M., Davisson, J.W. and Hass, M., KCl Single Crystals for 10.6 um Laser Windows, Navy Mater. Bull. 29-30, Mar. 1974.

5. Freiman, S.W., Mecholsky, J.J. and Rice, R.W., Fracture Analysis of ZnSe, Submitted to J. Am. Ceram. Soc.

6. Namjoshi, K.V., Bendow, B., Harrington, J.A., and Stierwalt, D.L., "Frequency dependence of multiphonon absorption in the transparent regime of fluoride crystals," Applied Physics Letters 26, 41 (1975).

TABLE OF CONTENTS

INTRODUCTION AND SUMMARY

Progress has continued toward our goals of understanding and diminishing absorption and increasing strength and toughness of alkali halides for laser windows. The emphasis of this ARPA program has continued to center on KCl as a viable candidate and a model for other halides, but work to transfer KCl technology to KBr has begun. Results of this program during this reporting period along with those of related Navy work are outlined below (see also the preceeding list of presentations and publications).

The growth of pure and alloyed, low loss ($\beta < 3 \times 10^{-4} cm^{-1}$) KCl crystals continued for in-house work, as well as for other investigators (e.g.13 crystals to 5 laboratories). KCl forging studies focused on better definition of the forging mechanisms to expedite transfer to other materials (e.g. KBr). These studies showed that the polycrystalline structure results from polygonization, the stages of which are directly related to the height reduction during forging. Studies of residual forging strain birefringence were augmented by computer mapping with a sensitivity of $\Delta n \sim 10^{-6}$ and a resolution of < 1 mm of refractive index changes. Initial results for press forged KCl confirm that low (e.g. $< 10^{-4}$) index variations can be achieved when forging above 250°C. Improvements in optical and mechanical properties of forged KCl were also indicated by laser tests where Sr^{+2} doped KCl forgings with low birefringence resisted permanent deformation and fracture for exposure times of $\geq \frac{1}{2}$ seconds at beam intensities of 20-30 KW/cm^2, and > 60 KW/cm^2 respectively.

Studies related to KBr will be reported in more detail in the next report. However, a technique for measuring lower absorption in the visible was adapted to the infrared region where a capability of measuring absorption coefficients in the $10^{-6} cm^{-1}$ range was shown for NaCl at 1.06 μm. Separation of surface and bulk absorption in a single measurement has been shown to be feasible by time-resolved calorimetry. Heat transfer calculations are being used to refine this technique with preliminary theoretical and experimental results showing good agreement. It is expected that both of

the above techniques (reported at the Tucson meeting) will shortly be applied to KBr crystals now being grown. Comprehensive theoretical evaluations (submitted for publication, only abstracts included in this report): 1) were made of the temperature and frequency dependence of multiphonon absorption of many halides using a Morse potential, and 2) showed that the form of the anharmonicity has a strong influence on absorption, the effect increasing with the order of the multiphonon process.

In related Navy studies, improved growth and polishing of NaF has resulted in lower 2-6 μm absorption and still greater reductions in vacuum UV absorption where surface losses are greater. In the course of the refinement of emittance techniques and study of 3-5 μm window materials, a 6 μm absorption band due to impurities was observed in several fluoride materials. In the area of other 10.6 μm materials, analysis of both fracture and slow crack growth in ZnSe showed that since failure is essentially controlled by flaws in single grains, 1) flaws are probably too small to be detected by NDT methods, and 2) higher proof stress ratios than those predicted by polycrystal fracture data are required.

In the remaining reporting period the growth and characterization of low loss KBr crystals will continue along with that of KCl. Absorption studies will center on refinement of measurement techniques for both lower loss materials such as KBr and separation of surface and bulk absorption. Mapping of refractive index changes in forgings will be incorporated with yield strength and fracture analysis and laser testing (which will include NWC-finished and-coated samples) in order to optimize press forged windows.

PRESS FORGED KCl: MICROSTRUCTURE DEVELOPMENT AND MECHANICAL AND OPTICAL PROPERTIES

P.F. Becher, S.W. Freiman
and
F.W. Patten
Naval Research Laboratory
Washington, D. C. 20375

1. INTRODUCTION

In order to produce pore-free polycrystalline materials of high optical quality, powder processing techniques have been avoided. Instead, hot working techniques have been employed where, by polygonization and recrystallization of a single crystal deformed primarily by $\{110\}\langle 1\bar{1}0\rangle$ slip, a dense polycrystalline material is obtained (1,2). These techniques not only produce stronger [σ_v>21 MN/m^2(>3000 psi)] polycrystalline materials but also yield optical properties such as absorption coefficients that are effectively controlled by the starting single crystals which are more readily optimized.

This section of the report summarizes two recent papers and presents initial results on quantitative measurement of refractive index variations in forgings. The first paper concerns recent results of the press forging of pure and strontium doped KCl single crystals with regard to microstructural development and consequent yield strength and fracture toughness.

The second paper treats the effects of test parameters, alloying, and microstructure on the fracture energy (i.e. toughness or resistance) of KCl.

2. RESULTS AND DISCUSSION

A. Forging Behavior and Microstructure

The deformation of unconstrained <100> axis KCl crystals, primarily by $\{110\}\langle 1\bar{1}0\rangle$ slip, exhibited a decrease in the work-hardening coefficient ($d\sigma/d\epsilon$) with increase in temperature, Fig. 1, most likely as a result of increasing secondary slip on {100}. The curves were characterized by two regions; namely, an initial rapid hardening stage (up to -0.2 to -0.3 true plastic strain) which decreases and becomes linear (Fig. 1). Strontium alloys exhibited much more distinct first stage with a higher hardening coefficient which again goes through a transition to a linear hardening stage (with a comparable coefficient to pure KCl) with increased strain. Also, strontium alloys required higher forging temperatures (>175°C) to maintain stress levels comparable to pure KCl as a result of increased resistance to dislocation motion from the divalent cation additions. Forging end face friction contributed in the form of an increasing hardening coefficient with increasing strain (generally $\geq$ -1.0 strain).

Initial substructure had little effect on the stress-strain behavior of unconstrained forgings. Forging along one <100> axis to -0.2 to -0.4 strain and annealing to form a polygonized structure, followed by a second forging along an orthogonal <010> axis to an additional -1.2 to -2.0 strain, yielded comparable stress-strain curves. The only difference in the reforging behavior was more rapid initial hardening which, like strontium alloying, gave rise to a more distinct transition to the linear hardening region with increasing strain. It is important to note from the above results that (1) the linear hardening coefficients above -0.3 strain are small [-7.6 to -20 MN/m^2 (-1.1 to -2.9 10^3 psi/in/in)], and (2) there are no obvious instantaneous or gradual stress drops with strain.

The microstructures developed after various forging strains in <100>

axis KCl crystals are represented in Fig. 1. Note that increasing the forging temperature had a minor effect resulting in a distinct "grain" structure at somewhat lower strains (1). Up to strains of ≈ -0.3 the substructure consisted of irregular dislocation arrays, which transform to a more defined and homogeneous polygonal-type substructure with increasing strain. The substructure or grain size appeared to be refined from ~15um at -0.3 to -0.4 strain to ~10um at -0.8 strain, probably by further network formation within grains. Above ~ -0.8 strain, a bimodal grain size was observed having large ($\geq$ 100um) grains in a fine-grained matrix. In fact, in pure KCl, "secondary recrystallization" of this type has often been observed after forging at room temperature (2). These large grains can be idiomorphic, exhibiting straight boundaries (Fig. 1) which x-ray data showed generally consisting of {100} surfaces. Strontium additions modified the microstructure in two ways, (1) higher forging temperatures were required to develop a polygonal structure, and (2) large grain formation was reduced (1).

The deformation behavior of unconstrained KCl indicated that recovery-polygonization processes strongly contribute to the forging microstructure. The lack of rapid workhardening with increasing strain (above -0.3) was consistent with Mecking and Kirch's analysis of dynamic recovery-recrystallization (3) where recovery and polygonization make major contributions. They considered the softening effects of recovery-polygonization and recrystallization during the deformation of metals and showed that the contribution of softening to the stress-strain behavior increases when going from recovery to polygonization to recrystallization as the dominant processes. In fact, these processes compete to lower the strain energy during

deformation, and recrystallization can be suppressed when the stored strain energy is diminished by recovery processes. The onset of recrystallization to form strain-free grains, as in single crystal copper, resulted in an actual rapid decrease in the true stress after rapid strain hardening under constant strain rate conditions. Polygonization can cause greater softening than recovery (by cross slip and annihilation) and decrease the work hardening rate more effectively. Thus, in KCl one suspected that softening by polygonization processes contributed significantly in maintaining a low linear hardening coefficient at strains between -0.3 to -1.0. Initial support for the importance of polygonization was indicated in limited anisothermal (25^{o} to 400^{o}C) scanning calorimetry studies of several low temperature (100^{o}C to 150^{o}C) KCl forgings where only a uniform evolution of heat was observed. Detectable exothermic peaks, typical of recrystallization, were not observed.

Polygonization has been generally visualized as predominating when slip occurs primarily on one plane and results in formation of subboundaries by dislocation climb processes. Note that the formation of parallel {110}slip bands in n<110> axis forgings and in each quadrant of <100> axis forgings was indicative of this. However, as described by Miekk-Oja and Lindroos (4), polygonization can be a more complex process, not necessarily so limited in the nature of slip or climb. They show that glide dislocations can be rapidly "knitted" into existing dislocation networks or forest dislocation in the presence of an applied stress.

The microstructure developed with increasing forging strain indicated that the irregular dislocation arrays introduced at low strains could act to form subgrain networks within deformation bands with the addition of

further dislocations by glide and climb. This resulted in a regular polygonal substructure which appeared to be further refined by formation of networks within these subgrains with further strain in the absence of recrystallization, as noted by calorimetry studies. The addition of strontium increased the temperature required to produce a "polycrystalline" microstructure, most likely by retarding dislocation climb and thus polygonization. Bernal G. et al (5) have also observed the breakup of rectilinear "grains" whose boundaries align with the deformation bands with increasing strain during hot rolling of KCl. This and the sharp crystallographic textures (6) and the Laue patterns observed in forged KCl were consistent with subgrain or grain formation by polygonization. Traskin et al (7) indicated that at very large reductions (~100%), complete recrystallization in KCl did not occur at temperatures below 300°C. In the present study, a decrease in the hardness of KCl forgings with > ~0.9 strain suggested localized recrystallization, which was supported by the inhomogeneous formation of large, often idiomorphic, grains. The microstructural stabilization by strontium additions may result from the suppression of recrystallization or reduction of the growth rate of these strain-free grains (8). The behavior in KCl was not unlike that of aluminum crystals which continuously polygonize with increasing strain until deformation results in sufficient stored energy to initiate recrystallization (3). Thus, the microstructure of KCl forgings resulted from the continued polygonization of dislocations primarily involved in $\{110\}\langle 1\bar{1}0\rangle$ slip. This led to the formation of well defined boundaries with increasing strain until local strain energy became sufficient to initiate recrystallization.

B. Fracture Toughness

While the fracture of alkali halide crystals by cleavage is well understood, little is known of inhibiting it (i.e., improving fracture toughness) in alloyed crystals. On the other hand, it has been established that the fracture resistance of KCl can be increased by hot working (1). Thus, this section reports on studies of the fracture toughness of alloyed KCl crystals in contrast to forged KCl.

The energy for propagation of {100} <010> cleavage cracks in strengthened KCl single crystals is dependent upon loading rate and mobile dislocation density at 22°C and 45% R. H. At a loading rate of 0.2 cm/min the fracture energy (γ_c) can lie anywhere within two limiting boundaries (Fig.1). For the lower boundary γ_c is independent of increasing yield strength (γ_c const. $\simeq$ 0.25 J/m^2) while the upper boundary $\gamma_c \propto \tau_y^2$ (τ_y is the resolved shear stress for {101} <10$\bar{1}$> slip; increased with divalent alloying or γ-irradiation) such that at $\tau_y \simeq$ 9MN/m^2, γ_c = 4 J/m^2. Low γ_c values are due to a lack of crack tip blunting by {101} <101> dislocation motion away from the crack tip region. Higher γ_c values result from blunting of varying lengths of the crack front. Further increases in γ_c are limited by dislocation motion into the crack tip region which increases the crack tip strain energy and causes the crack to propagate. This dependence on dislocation motion is described by a second power dependence τ_y of γ_c. The range of fracture toughness values at a given strengthening (τ_y) level is attributed to a lack of mobile dislocations in the crack tip region. Prestraining low yield strength KCl crystals (1% permanent strain), to obtain mobile dislocations prior to introducing a precrack, results in average γ_c values falling near the upper boundary.

At faster loading rates (5 cm/min) the γ_c values of strengthened crystals are consistently in the range of 0.25 to 0.35 J/m^2 indicative of insufficient dislocation mobility. At slower loading rates (0.02 cm/min) the extensive degree of plastic deformation that occurs at very low stresses negates crack propagation in "pure" KCl crystals.

The point is that strengthened KCl single crystals are not necessarily any more resistant to fracture than pure crystals and their toughness is quite dependent upon loading rate and mobile dislocation density.

On the other hand, hot worked KCl, both pure and alloyed, has consistently high fracture toughness (γ_c = 3.2 to 4.5 J/m^2) at 0.2 cm/min loading rate, as well as high yield strengths (Fig. 1). Because of the consistently high γ_c values of hot worked KCl, it is expected that it may also be less sensitive to reloading rate. The explanation for the high fracture toughness of these materials is the influence of a high density of mobile dislocations, as well as the presence of subgrain boundaries, on crack tip blunting. It should be noted that forged bodies exhibit psuedo cleavage fracture with little change in crack plane (generally slightly curvilinear but following a {100} texture path). Therefore, the consistently high toughness is primarily related to dislocation crack tip blunting rather than gross changes in crack path.

C. Residual Forging Strain Effects

Since the improved strength of hot worked KCl is often accompanied by increased residual strain birefringence and associated optical inhomogeneity, attention has been directed at improving its optical quality. Thus, the influence of forging temperature on both strength and optical homogeneity

of forgings is also discussed.

As discussed earlier (1) divalent alloying results not only in solid solution strengthening but also enhanced strengthening from residual forging strains remaining after forging at $\leq 200^{o}C$. Additional studies (10,11) have shown that the strength of press forged alloyed KCl is dependent upon forging temperature. With an increase in forging temperature above $200^{o}C$ the as-forged yield strengths of strontium doped KCl decrease (9b). This decrease in strength is seen as a result of the recovery of residual forging strains. Although the polycrystalline-like deformation microstructure of hot worked KCl results from rapid polygonization of the dislocations introduced during hot working into cell walls, alloying inhibits complete recovery and polygonization of these dislocations at forging height reduction of up to 50 to 70+%. Thus higher forging temperatures are required to completely polygonize the structure, as well as introduce sufficient secondary slip to eliminate the residual forging strains.

At the same time, observations of forgings with transmitted polarized light have shown that increasing forging temperatures result in a decrease in {110} birefringence bands such that at $T > 250^{o}C$ these are virtually eliminated (9b). The removal of these bands coincides with the reduction in as-forged yield strength indicating that elimination of the residual strain associated with the banding is responsible for strength losses.

A more sensitive measurement of stress-induced birefringence in forgings has been attempted by scanning a polarized helium-neon laser beam across the sample and analyzing the transmitted light using a high-sensitivity photodiode detector. These data points were collated and printed on a Calcomp computer peripheral as a three dimensional simulation of refractive

index changes ($\Delta\eta$) across the sample. Such a mapping with a 1mmX1mm grid is shown in Fig. 3, compared to the view normally observed between crossed polarizors. The resolution of $\Delta\eta$ is about 10^{-6}, based on normal computations for crossed linear polarizors and the noise level of the laser employed. In this case, the linear polarizer-analyzer combination was oriented at 45° to the sample edges. Currently the apparatus is being modified to accomplish the same measurement in circularly polarized light as the crystal or forging orientation is invariant and $\Delta\eta$ values are not influenced by the angle of polarization.

The birefringence banding in forgings and associated residual strain effects on yeild strength, enhanced 10.6μm irradiation (6 mm dia., 19kw/cm^2, top head beam) damage in the form of plastic deformation, particularly when intersecting banding occurs. Such damage is diminished when the yield strength of the forged bodies is increased above 3000 psi (12). Thus selection of forging temperature for windows should be considered to optimize the birefringence inhomogeneities and yield strength and thus improve the damage resistance of the bulk window material.

3. SUMMARY

The microstructure of forged pure KCl at height reduction of $\leq$60% ($\leq$ -0.9 plastic strain) is a result of simultaneous $\{110\}\langle 1\bar{1}0\rangle$ slip and polygonization. A "grain" structure is initially formed at strains > -0.3 and is refined to ≈10um with increasing strain with only a minor influence of forging temperature in the range of 125° to 200°C. At strains > -0.9, inhomogeneous recrystallization is initiated and grains are nucleated which grow rapidly into the surrounding strained, fine-grained matrix. KCl

forgings exhibit strong textures, but also show improved strength fracture toughness. This indicates that even though polygonized structures would contain low angle boundaries, there is sufficient boundary misorientation to affect mechanical properties. The strontium alloys, although requiring higher forging temperatures, have very stable fine-grained microstructures, as well as improved strengths, due to solid solution hardening, which can be augmented by strain hardening.

The resistance to fracture in KCl is consistently improved by hot working (γ_c= 2 to 4 J/cm^2) while strengthened crystals exhibit very variable toughness (γ_c= 0.5 to 4 J.m^2) dependent not only on the yield stress but also on strain rate and specimen dislocation content. The toughness of hot worked KCl is related to the ease of crack tip blunting; a result of the propensity of dislocation sources in these bodies. Thus, strengthened crystals might be toughened somewhat by prestraining to introduce mobile dislocations as initial studies indicate.

By raising forging temperatures, residual strain birefringence is diminished with a resultant improvement in optical homogeneity. There is some accompanying loss in yield strength. But alloying, which stabilizes the fine grained microstructure, improves strength and appears promising for optimizing strength and optical quality. Thus, in small scale windows of alloyed KCl, yield strengths of 4000 to 5000 psi and negligible birefringence have been achieved.

ACKNOWLEDGMENTS

The research was supported by the Advanced Research Projects Agency of the Department of Defense and was monitored by Dr. C. M. Stickley under

ARPA Order No. 2031. The contributions of Dr. M. Krulfeld and Mr. W. L. Newell of NRL in portions of the experimental work are acknowledged, as are discussions with Drs. B. G. Koepke of Honeywell Corporation Research Center and H. K. Bowen of M.I.T.

REFERENCES

1. P.F. Becher, S.W. Freiman, P.H. Klein and R.W. Rice, Proc. Conf. High Power Infrared Laser Window Materials, Vol. II, pp. 579-600 (1974), C.A. Pitha, A. Armington and H. Posen (eds.) AFCRL-TR-74-0085.

2. B.G. Koepke, R.H. Anderson, E. Bernal G. and R.J. Stokes, J. Appl. Phys. 45, 969 (1974).

3. H. Mecking and F. Kirch, pp. 257-288 in Recrystallization of Metallic Materials, F. Haessner (ed.), Dr. Riederer-Verlag GmbH, Stuttgart (1971).

4. H.M. Miekk-Oja and V.K. Lindroos, Surf. Sci. 31, 442 (1972).

5. B.G. Koepke, R.H. Anderson and E. Bernal G., pp. 601-614 in Proc. Third Conf. on High Power Infrared Laser Window Materials, Vol. II, C.A. Pitha, A. Armington and H. Posen (eds.), AFCRL-TR-74-0085 (1974).

6. E. Bernal G., B.G. Koepke, R.H. Anderson and R.J. Stokes, Preparation and Characterization of Polycrystalline Halides for Use in High Power Laser Windows, Quart. Tech. Report No. 3, Corporate Research Center, Honeywell, Inc., December, 1972.

7. V. Yu. Traskin, Z.N. Skvortsova, N.V. Pertsov and E.D. Shchukin, Soviet Phys. Cryst. 15 733 (1971).

8. M.F. Yan, R.M. Cannon, H.K. Bowen and R.L. Coble, in Deformation of Ceramics, R.C. Bradt and R. Tressler (eds.) Plenum Press (In Press) (1974).

9. (a) S.W. Freiman, P.F. Becher and P.H. Klein, submitted to Phil. Mag.

(b) S.W. Freiman, P.F. Becher and P.H. Klein, High Energy Laser Windows, Semi-Annual Report 4, ARPA Order 2031, U.S. Naval Research Laboratory (1974)

10. P.F. Becher, R.W. Rice and M. Krulfeld, High Energy Laser Windows, Semi-Annual Report 4 (1974), ARPA Order 2031, U. S. Naval Research Laboratory.

11. G.D. Hendrickson, J.E. Starling and W.B. Harrison, Halide Material Processing for High Power Laser Windows, Interim Report 5 (1973), AFML Contract F33615-72-C-2019, Honeywell, Inc.

12. P.F. Becher, J.J. Mecholsky, J.R. Spann, and R.W. Rice, Proc. 4th Conf. High Power Infrared Laser Window Materials (1974).

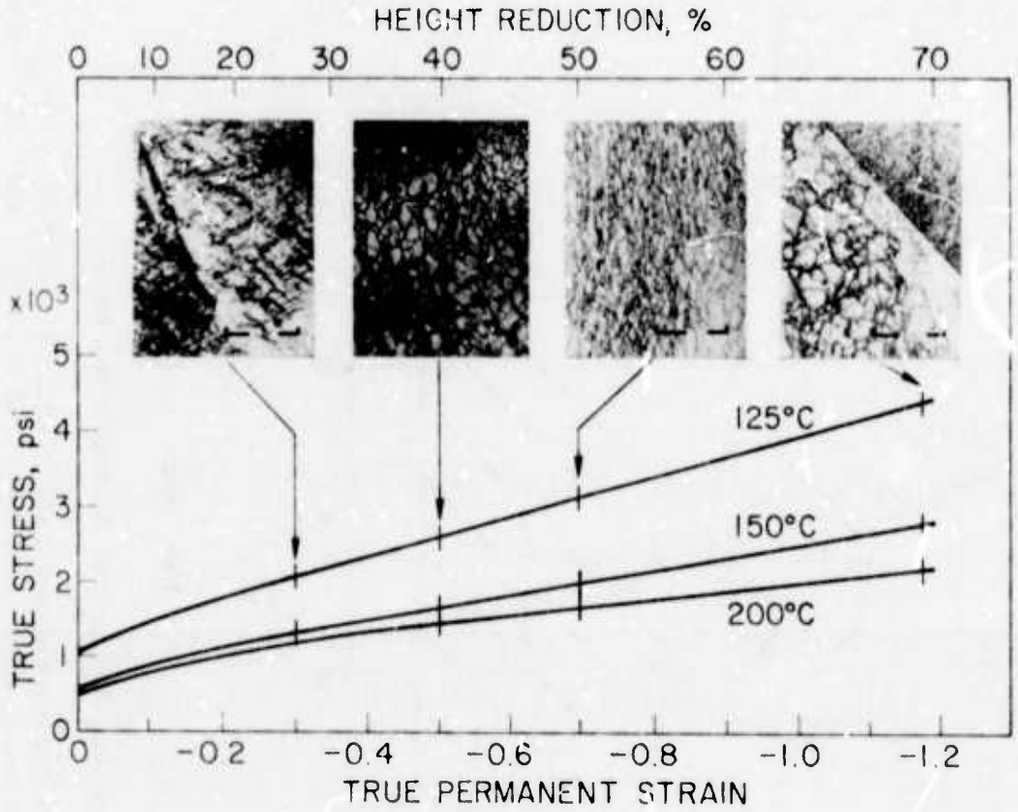

Figure 1. Deformation During Forging of Unconstrained <100> KCl and Resultant Microstructure. (Bar on micrographs = 100 μm.)

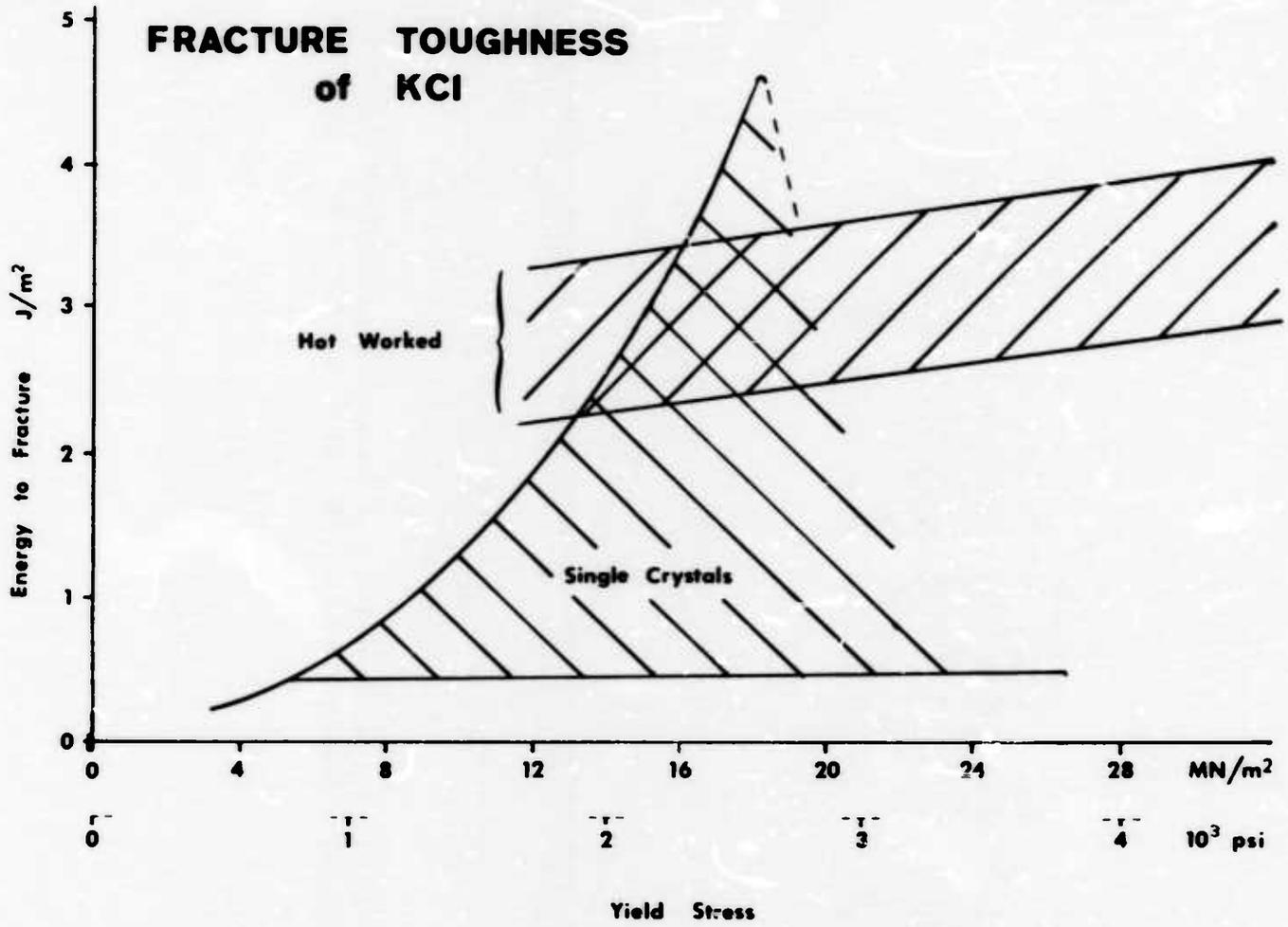

Figure 2. Critical Fracture Energy for Strengthened KCl.

Samples were precracked and tested at 22°C, 45% R.H. with crystals loaded at deflection rates of 2×10^{-1}, 5 and 2×10^{-2}cm/min. and hot worked specimens at 2×10^{-1}cm/min.

(a)

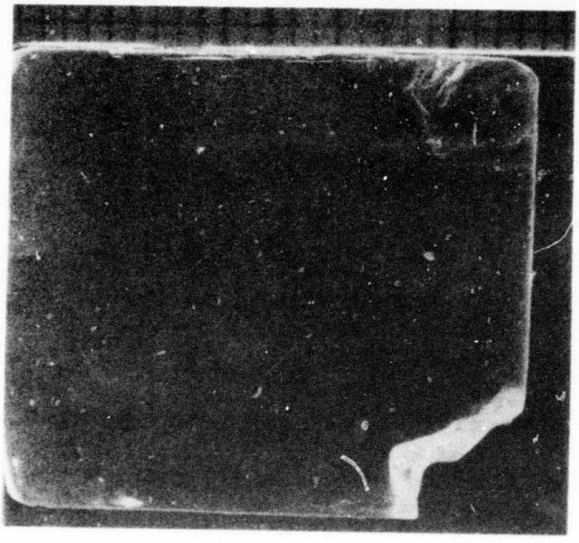

(b)

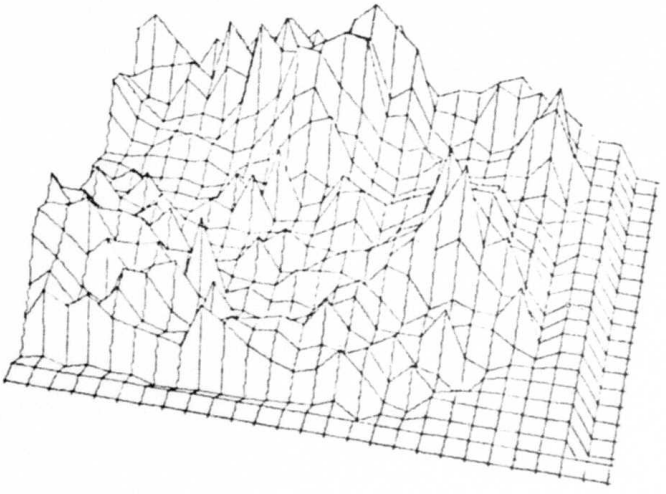

Figure 3. Strain Birefringence in Press Forged KCl.

a) Photograph of forging between crossed polarizors and
b) three-dimensional mapping of index changes using a laser polarimeter as explained in the text with a 1mm grid. The scale is approximately the same in both views.

SUMMARY OF 10.6 MICRON LASER TESTING OF UNCOATED KCL

P. F. Becher, J. J. Mecholsky, J. J. Spann
and
R. W. Rice
U. S. Naval Research Lab.
Washington, D. C. 20375

1. INTRODUCTION

Several laser tests of uncoated samples of both KCL single crystals and press forged KCL have been made. The purpose of these tests has been to provide a base line for material development, i.e. to establish 1) where we are in the resistance of KCL materials to gross laser damage, and 2) the response of the bulk laser window materials for comparison with possible subsequent testing of finished and coated KCL laser window samples (in cooperation with H. Bennett and colleagues at NWC). This section will briefly summarize all past tests; for greater detail the reader is referred to a recent paper[1].

2. EXPERIMENTAL

Samples were irradiated with the laser beam at an angle of approximately 10^{o} off the surface normal, so that the window could be simultaneously observed in transmitted circular polarized visible light with a high speed movie camera. This provides information on any microscopic changes in birefringence, crack development and crack growth during the test. Samples were also optically examined before and after irradiation. An important aspect of these tests is that the sample size was controlled so that the ratio of the beam area to the sample area was never less than approximately 25%. This was done in order to minimize the overestimates of damage

thresholds that can occur with small beams in large samples.

3. RESULTS AND DISCUSSION

Earlier laser tests were with a "top hat" beam; i.e. average and peak power densities the same. The first tests with power densities of approximately 13 KW/cm^2 showed that commercial single crystals and press forged materials at that time either underwent extensive plastic deformation or fracturing from pre-existing cracks while being irradiated for a few seconds. Such samples were characterized by total absorptions of $\geq 10^{-3}$ cm. and substantial birefringence especially in the press forged materials. Subsequent testing at power densities of 19 KW/cm^2 showed that improved single crystals and press forged materials having total absorptions of $\leq 10^{-3}$ cm. and substantially reduced birefringence exhibit some local plastic deformation in a few seconds if their yield stresses were too low. However, samples with suitably high yield stress, i.e. greater than 3000 PSI, transmitted such power densities for 6 seconds or more with no observable effects. Further, some press forged samples exhibiting no observable effects had pre-existing cracks in them which did not propagate during the laser irradiation demonstrating both the reduction in laser induced stresses in these materials as well as the effect of the high fracture toughness in the press forged material.

In order to perform tests at higher power densities and yet maintain a reasonable beam area required use of a second laser system. This system is more difficult to maintain accurate control of the power density from run to run and it has substantial inhomogeneity in the beam which is likely to be characteristic of many laser systems for which windows will be used. It

is not uncommon for peak power densities to occur over small but measureable areas which will be as much as 10 fold greater than the average power density. Thus tests at substantially higher power densities than the average anticipated usage are important to insure that no damage will occur from such high power density peaks. Tests with this second laser again confirm that lower yield stress materials such as single crystals will undergo extensive plastic deformation during transmission of power densities of the order of a few tens of KW/cm^2 for a few seconds or less. They also again demonstrate that press forged materials having suitable yield stresses and fracture toughnesses can withstand such power densities without deformation or fracture. Limited amounts of plastic deformation appear to only occur in the region of peak power densities $> 30\ KW/cm^2$. Small cracks typically developed in the region of high power density only above power densities above 60 KW/cm^2 and typically cracking was confined only to the region of high power densities, again testifying to the toughness of press forged materials inhibiting crack propagation. Further, the times for either plastic deformation or fracturing to occur at the above respective power density regimes are of the order of 1/2 sec. or more. Thus, while substantial further work is needed to bring optical distortion levels to the range desired, these tests show that substantial progress has been made in developing materials to resist gross damage from the high power densities expected in some regions found in laser beams which are of interest.

Reference

1. Becher, P.F., Mecholsky, J.J., Spann, J.R. and Rice, R.W., Laser Testing of Uncoated KCl, to be published in Proc. 4th Laser Window Materials Conf., Tucson, Ariz., Nov. 1974.

MULTIPHONON ABSORPTION IN IONIC CRYSTALS*

L.L. Boyer, James A. Harrington,†
Marvin Hass, and Herbert B. Rosenstock
Naval Research Laboratory
Washington, D. C. 20375

ABSTRACT

Calculations of the frequency and temperature dependence of infrared multiphonon absorption for many alkali halides and alkaline earth fluorides have been completed and compared with previously published data. The temperature dependence of the infrared absorption, of pure crystals of NaF, NaCl, and KCl at 10.6 μm from room temperature to close to the melting point has also been determined. The calculations are based upon a simple approach involving an interatomic Morse potential function in which lattice dispersion is introduced via a multiphonon frequency distribution. Good agreement between experiment and theory is obtained in which the "observed" lattice density-of-states and thermal expansion coefficient data (which determines the degree of anharmonicity) are the principal input to the calculations. Some structure in the multiphonon spectrum is predicted for some compounds at low temperatures, which has not yet been observed experimentally. Since the Morse potential has an exact quantum mechanical solution, the anharmonicity is contained in the calculations without resorting to perturbation theory.

---

* Complete article to be published in Phys. Rev. Mar. 1975

† Now at University of Alabama - Huntsville,

MULTIPHONON ABSORPTION STUDIES

Alfred Nedoluha,
Naval Electronics Laboratory Center
San Diego, California

In previous theories of anharmonic multiphonon absorption, different approaches have utilized different forms of the anharmonic potential (Huggins-Mayer potential for perturbation theory, Morse potential for rigorous solution of the cell model, etc.), but no systematic attempt has been made to investigate the quantitative differences due to different forms of the anharmonicity. In the present work, one approach (perturbation theory) has been chosen, and the absorption coefficients resulting from different forms of the anharmonicity have been compared. One of the results of this work is that the form of the anharmonic potential has a strong effect on the magnitude of the absorption and that this effect increases with increasing order of the multiphonon process.

An abstract of this work is given below; the full manuscript will appear in the Proceedings of the Conference on Optical Properties of Highly Transparent Solids (Waterville Valley, 1975) and in the next ARPA Progress Report.

Multiphonon absorption in KCl has been calculated by the use of perturbation theory (including vertex corrections) for four forms of the Born potential: (1) inverse power, (2) exponential, (3) exponential with preexponential power factor, and (4) Morse potential. The one-phonon density of states is approximated by a Debye model; the n-phonon density (including occupation probability for each phonon) is calculated

analytically without resorting to the central limit theorem. Measured values of the temperature dependent lattice constant and phonon frequencies have been employed. Depending on the chosen form of the Born potential, the calculated 10.6μm absorption values at 300K differ from each other by more than two orders of magnitude. Without parameter adjustment, the inverse power potential gives good agreement with emittance data over the whole observed frequency range of intrinsic multiphonon absorption at 77K, 273K, and 373K, while potentials (2) to (4) give absorption values which are too low. Above 500K, laser data at 10.6μm fall below the values calculated from potential (1). The same theory has been applied to predict multiphonon absorption in KI.

Growth, Surface Finishing, and Optical Characterization of Sodium Fluoride and Other Fluoride Laser Window Crystals

Philipp H. Klein and James W. Davisson

U.S. Naval Research Laboratory
Washington, D.C. 20375

Abstract

Sodium fluoride and alkaline-earth fluorides have many properties which commend them for consideration as window materials for molecular fluoride lasers. Their absorption coefficients are low at the HF and DF laser wavelengths, they have good mechanical properties, and they are tolerant to atmospheric moisture. The lower melting point of NaF and its greater ease of purification have permitted its use in solving many handling problems which are common to all fluorides.

For sodium fluoride, fractional recrystallization and fractionation during Czochralski growth of crystals has reduced the hydroxyl concentration to 0.07 OH^- per million anions. This has rendered the absorption at 2.7 μm undetectable by spectrophotometric methods. This absorption band is ascribed to OH^- and other oxygen-containing structures, and interferes directly with HF laser emission lines. Infrared absorption measurements on our NaF give extrapolated absorption coefficients of 3×10^{-6} cm^{-1} at 5 μm and 2×10^{-9} cm^{-1} at 3.8 μm.

Aluminum oxide (Linde A) in 2-propanol is effective for mechanical polishing of NaF. No surface hydroxyl absorption is introduced by this method. Chemical polishing with dilute manganous-ion solutions containing small amounts of HF improves optical transmission by diminishing surface absorption.

Commercially-prepared crystals of calcium, strontium, and barium fluoride were used in chemical-polishing studies. Acid solutions were found to etch the surfaces of calcium and strontium fluorides. Widening of surface scratches by means of polishing action was achieved in barium fluoride. The quality of mechanically-polished surfaces of alkaline-earth fluorides was not improved by any of the mixtures investigated.

1. INTRODUCTION

Sodium fluoride and the alkaline-earth fluorides are potentially useful as laser windows in the wavelength region between 2 μm and 6 μm (1). By extrapolation of measurements (2,3) and of theoretical results (4), these candidate window materials can be shown to have intrinsic absorption coefficients ranging from 10^{-4} cm^{-1} to 10^{-9} cm^{-1} in the 2-6 μm region. As fluorides with low refractive indices and acceptable mechanical properties, they are of particular interest for use in conjunction with HF and DF lasers.

To benefit from low intrinsic absorption within a window, it is essential that sources of extrinsic absorption be excluded, and that absorption and scattering at the surface be reduced to a minimun. Hydroxyl-ion contamination in commercial NaF crystals poses serious problems. Presence of OH^- results in absorption lines close to the output wavelength of HF lasers. We describe here the removal of OH^- to eliminate these interfering absorption lines. We also describe our effective use of chemical polishing methods for removal of damage and contamination from the surface of NaF crystals.

Commercially-prepared calcium fluoride, strontium fluoride, and barium fluoride crystals are relatively free of hydroxyl contamination. We used these commercial crystals in our preliminary studies of chemical polishing of these compounds, reported here.

2. SODIUM FLUORIDE

A. Purification In the 2-6 μm region, extrinsic absorption in purified NaF is primarily due to the presence of OH^- (5). Complexes of OH^- with divalent metals and other oxygen-containing impurities may also produce extrinsic absorption (6). When OH^- concentrations are less than 1 per million anions (1 part per million atomic, or 1 ppmA), metallic impurities may be tolerated in cationic concentrations of 10^{-5} to 10^{-6} (1-10 ppmA). Prevention of contamination by OH^- is therefore desirable.

The main source of hydroxyl contamination in NaF is simple hydrolysis:

$$NaF + H_2O = NaOH + HF$$

Atmospheric moisture is sufficient to introduce detectable amounts of NaOH. Because HF is volatile, it escapes and "locks in" the hydroxyl contamination. We have found it

most effective (7) to prevent hydrolysis by converting NaF to $NaHF_2$ in HF solution, recrystallizing and drying the $NaHF_2$, and then expelling the HF at temperatures above 200 C. Titanium-gettered argon is used as the atmosphere here and in crystal growth.

Even when these precautions have been taken, some absorption may be seen in the 2.6-2.7 μm region. As is shown in Figure 1, when parts of Czochralski-pulled crystals are used as the raw material for "second generation" crystals, the absorption is diminished below the limits of spectrophotometric detection.

In order to measure small residues of OH^- in NaF, we have found it most convenient to make use of the high oscillator strength of OH^- in the vacuum ultraviolet (VUV) portion of the spectrum. At 151 nm, presence of 0.7 ppmA of OH^- results in an absorption coefficient of 1 cm^{-1} (5). With the aid of VUV spectrophotometry, we have measured OH^- concentrations of about 1-5 ppmA in first-generation boules and 0.07-0.10 ppmA in second-generation crystals.

Absorption measurements as a function of length in the 120-180-nm region have shown that surface absorption makes a negligible contribution at wavelengths greater than 170 nm. Surface absorption increases monotonically at shorter wavelengths, so that as much as 30-40 per cent of incident 135-nm light may be absorbed at the surface (3). No enhancement of surface absorption was detected at 151 nm, even after days of exposure to moist air. We conclude that surface hydrolysis is insignificant in NaF crystals exposed to room atmospheres. On the other hand, surface condition - presence of scratches, pits or other defects - has a profound effect on the VUV absorption spectrum. We have used this fact in demonstrating the efficacy of chemical polishes.

B. Chemical Polishing Sodium fluoride can readily be polished mechanically with the aid of aluminum oxide (Linde A), using 2-propanol as a lubricant. "Scratch-free" surfaces are attainable with some patience. In Figure 2, we show a residual scratch and its removal with the aid of a chemical polishing solution (40 ml of 0.051% $Mn(NO_3)_2$ + 3 drops of concentrated HF) derived from an etchant (8). True polishing is shown: defects are broadened and interrupted layers of the surface are removed, finally exposing a fresh surface which is free of sharp discontinuities at 320-power magnification.

Effects of chemical polishing on the VUV absorption spectrum are shown in Figure 3. It is noteworthy that the small absorption peak at 141 nm disappears after the specimen is chemically polished. This absorption line has been ascribed to the presence of the O_2^- ion, although the evidence is not conclusive (9). Assuming that the assignment is correct, removal of O_2^- from the surface is a desirable result because of its association with infrared absorption.

The dashed line in Figure 3 represents the surface absorption of a mechanically polished crystal of NaF, determined from absorption measurements as a function of length (3). Chemical polishing is seen to be most effective at precisely those VUV wavelengths at which surface absorption is large.

The total absorption of our NaF crystals between 2 μm and 6 μm is so small that surface absorption is not readily detected with the spectrophotometer. Nevertheless, removal of VUV-detectible surface defects can only increase infrared transmission, since small flaws are not detected at longer wavelengths. Laser-calorimetric measurements will be required in order to measure quantitatively the surface absorption of chemically-polished NaF in the 2-6 μm region.

3. ALKALINE-EARTH FLUORIDES

Properties pertaining to the use of alkaline-earth fluorides as 2-6 μm windows have been summarized by Sparks and Chow (1). We have verified spectrophotometrically the low 2-6 μm absorption of commercially-prepared crystals (obtained from Optovac, Inc., North Brookfield, Massachusetts 05135). We have also made a few VUV measurements on mechanically-polished samples as functions of length. These have led us to conclude that VUV absorption after polishing with Linde A alumina in 2-propanol is much smaller than is the case with NaF.

In view of the demonstrated small bulk absorption in the infrared and the indication that surface absorption may also be small, requirements for a chemical polish for these compounds are somewhat relaxed. The principal effect sought from a chemical polish is that it remove debris and residual scratches left by mechanical polishing and that it do this without destroying the smoothness and flatness of the surface. As shown below, this has been more difficult to achieve with the alkaline-earth fluorides than with sodium fluoride.

A. Calcium Fluoride Solutions investigated in the past as polishes for calcium fluoride are really dislocation etchants. A true chemical polish does not produce dislocation etch pits. Nevertheless, it has been shown (10) that a dislocation etchant can be used as a "pseudopolish" if it is used for times so short that scratches are enlarged but that macroscopic etch pits are not formed. In this regard, our experience has shown that all the acid solutions we have investigated (including hydrochloric, sulfuric, acetic, and phosphoric acids and many of their mixutres) have yielded dislocation etch pits on calcium fluoride. We show such etch pits in Figure 4A. This freshly-mixed warm solution had been found (10) to be a true chemical polish. We cannot explain the difference in behavior.

B. Strontium Fluoride We agree with a previous investigation (10) that the surface of strontium fluoride is unstable in acid solutions and yields a heavily-pitted surface, shown in Figure 4B. Clearly, no useful chemical polishing solution has been evolved for this material.

C. Barium Fluoride Of all the alkaline-earth fluorides, only barium fluoride did not show immediate evidence of dislocation etch pits when we attempted to polish it chemically. Our results (see Figure 5) suggest that water may be a necessary ingredient of any effective polishing solution.

4. CONCLUSIONS

We have demonstrated that sodium fluoride can be purified of major sources of extrinsic absorption between 2 and 6 μm, and that it can be prepared in the form of chemically-polished, single-crystal specimens. Laser calorimetry will be required in order to obtain precise infrared absorption data.

Although our VUV measurements of alkaline-earth fluorides show that mechanical polishing produces little surface absorption, we have not yet evolved a chemical polish which removes fine scratches in these materials. As with NaF, laser calorimetry is needed to obtain precise infrared absorption data.

5. REFERENCES

1. See, for example, Sparks, M., and Chow, H. C., "High-Power 2- to 6-μm Window Material Figures of Merit with Edge Cooling and Surface Absorption Included," J. Appl. Phys. 45, 1510-1517, (1974).

2. Deutsch, T. F., "Absorption Coefficients of Infrared Laser Window Materials," J. Phys. Chem. Solids 34, 2091-2104 (1973).

3. Klein, P. H., Krulfeld, M., and Claffy, E. W., "Impurity Effects on Vacuum-Ultraviolet and Infrared Multiphonon Spectra of Laser-Window Materials," from High Energy Laser Windows: Semi-Annual Report No. 4, ARPA Order 2031, Naval Research Laboratory, 30 June 1974, pp. 59-74.

4. Boyer, L. L., Harrington, J. A., Hass, M., and Rosenstock, H., "Multiphonon Absorption in Laser Window Materials," presented at Fourth Laser Window Conference, Tucson, Arizona, 18-20 November 1974.

5. Meistrich, M. L., "U.V. and I.R. Absorption in OH^--Doped NaF," J. Phys. Chem. Solids 29, 1119-1125 (1968).

6. Stoebe, T. G., "Distribution of Hydroxide Ions in Doped Alkali Halide Crystals," ibid. 31, 1291-1294 (1970).

7. Klein, P. H., Claffy, E. W., and Collins, W. C., "Purification, Crystal Growth, and Evaluation of NaF for Low-Loss Windows and Optical Information Storage," presented at Conference on Preparation and Properties of Electronic Materials, Electronic Materials Committee, The Metallurgical Society of AIME, Boston, Massachusetts, 9-11 September 1974; to be published.

8. Davisson, J. W., and Levinson, S., "Selective Etch for New Edge Dislocations in Sodium Fluoride," J. Appl. Phys. 37, 4888-4894 (1966).

9. Meistrich, M. L., "ESR and Optical Studies of O_2^- in NaF," J. Phys. Chem. Solids 29, 1111-1118 (1968).

10. Harrington, J. A., "Low Loss Window Materials for Chemical Lasers: Semi-Annual Technical Report, ARPA Order 2614, The University of Alabama in Huntsville, July 1974, pp. 3-14.

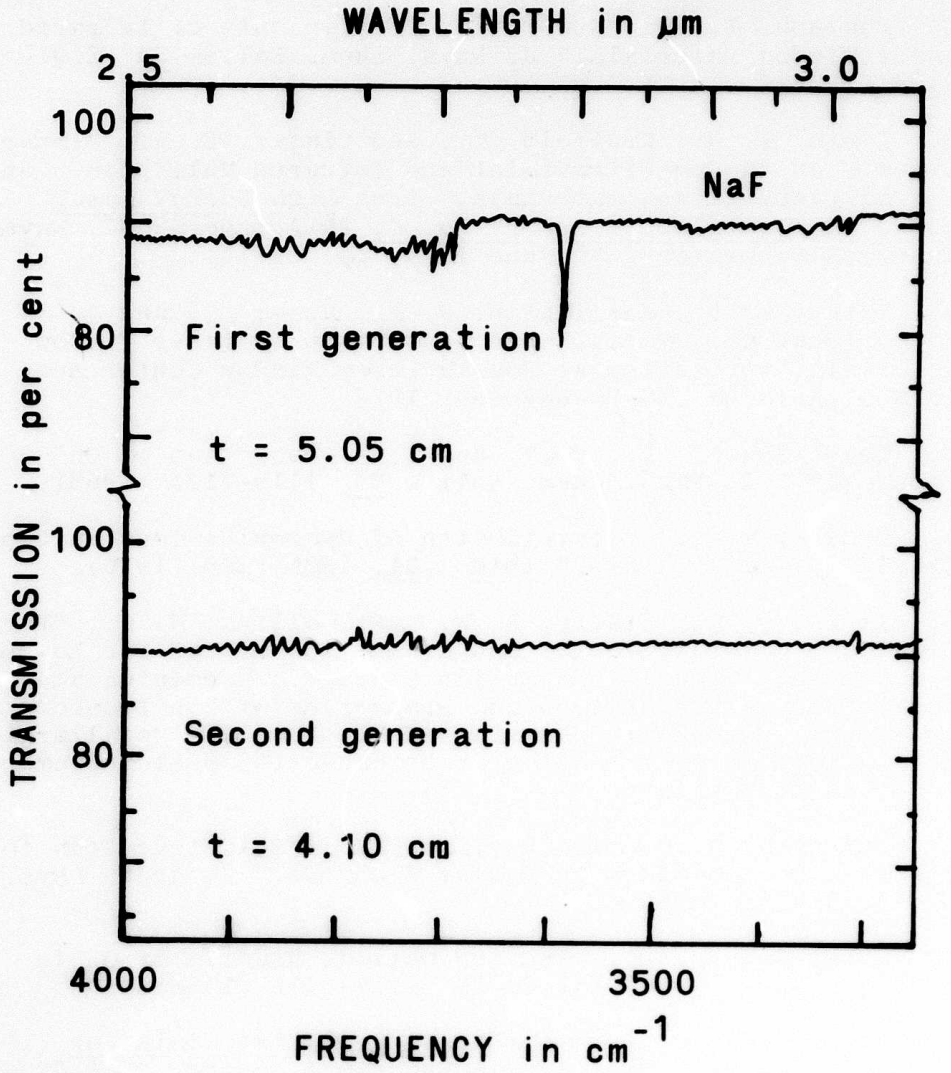

Figure 1. Infrared absorption spectra of sodium fluoride crystals in the region containing the principal OH^- absorption lines. The sharp-line absorption at 2.78 μm is due to complexes formed between OH^- and divalent impurity ions (Ref. 5). The absorption constant at 2.78 μm (0.03 cm^{-1}) corresponds to a OH^--complex concentration in the first-generation crystal which is about one-fourth that in second-generation crystals of Reference 5. The spectrum of the second-generation crystal shows no evidence of the presence of OH^- or its complexes.

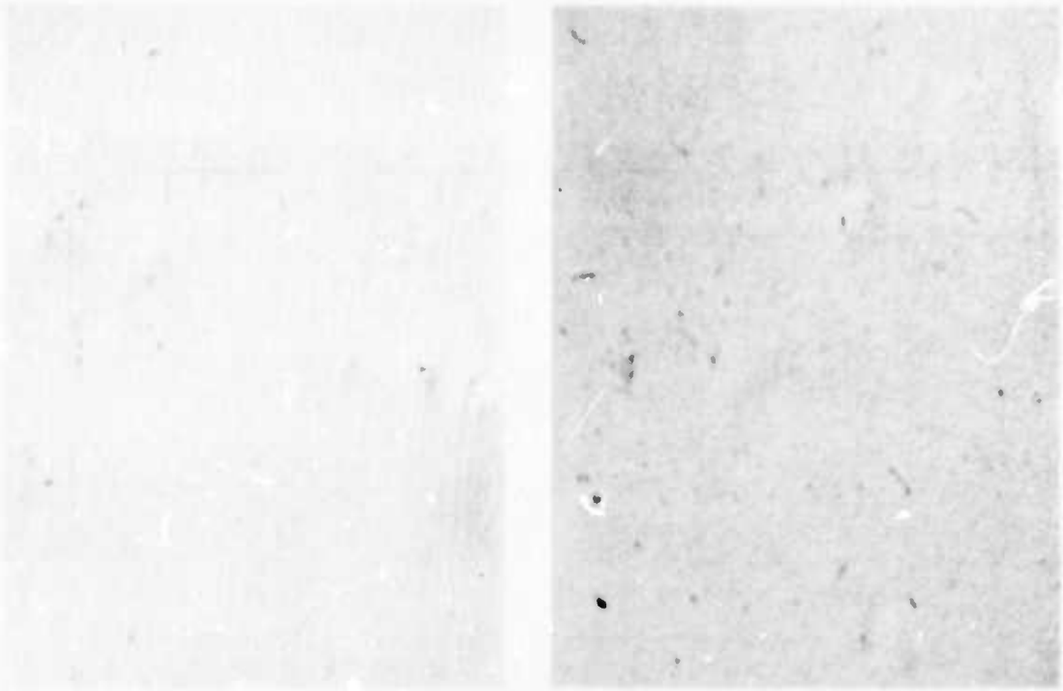

(a) (b)

Figure 2. Polishing of sodium fluoride. A: Mechanical polish with alumina (Linde A) and ethanol, showing digs and scratches. B: After 1 minute in 40 ml of 0.05% manganous nitrate solution containing 3 drops of 48% HF. Surface artifacts have been removed. Nomarski photomicrographs, 320X.

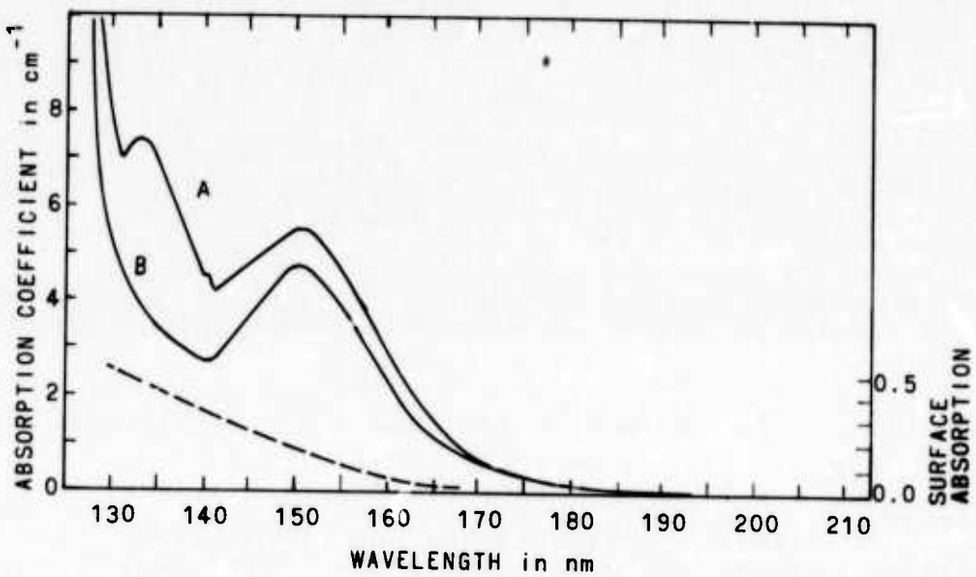

Figure 3. Vacuum-ultraviolet spectra of sodium fluoride. A: Mechanical polish with Linde A + 2-propanol. B. Chemical polish with solution described above. Dashed line (righthand ordinate) gives surface absorption determined in another series of measurements. Hydroxyl concentration in these first-generation crystals is about 3-5 ppmA determined from 151-nm peak.

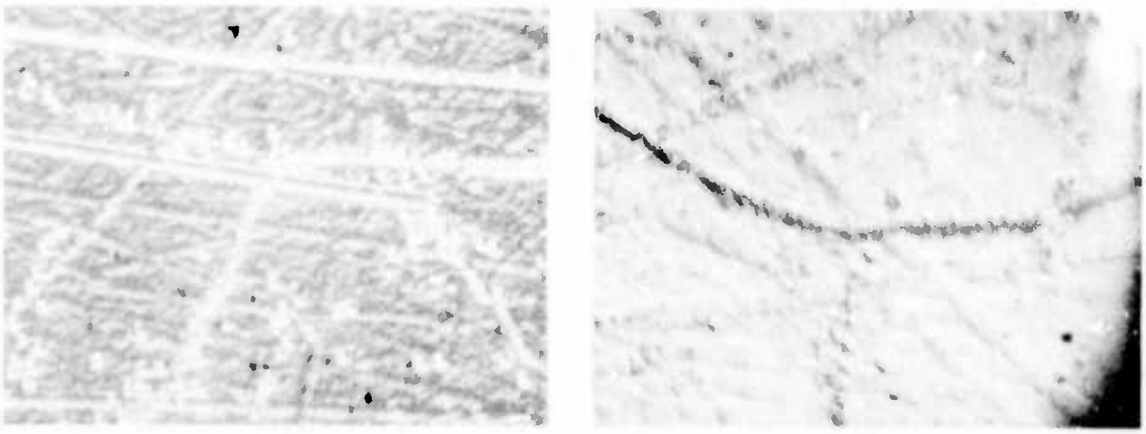

(a) (b)

Figure 4. Dissolution of cleavage faces of alkaline-earth fluorides. A: CaF_2 in warm, fresh 3 H_2SO_4 : 2 $HC_2H_3O_2$ for 20 minutes. Grain walls and random dislocation etch pits are clearly visible. B: SrF_2 in 4 HCl : 1 H_2O solution for 10 minutes. Nomarski micrographs, originally 320X.

(a) (b) (c) (d)

Figure 5. Dissolution of barium fluoride. A: Polished with Linde A and ethanol. B: Same region as A, immersed for 5 hours in 4 H_2SO_4 : 9 $HC_2H_3O_2$. Fine scratches have been exposed, but no effective polishing action can be seen. No further change occurred after 20 additional hours' immersion. C: Same specimen, repolished with Linde A and ethanol. D: Surface of C after 10 minutes in distilled water. Fine scratches have been exposed, much as in B. After 20 additional hours' immersion, the surface became irregular, indicating that the dissolution process continues.

SPECTRAL EMITTANCE OF FLUORIDE LASER WINDOW CRYSTALS

D. L. Stierwalt,
Naval Electronics Laboratory Center,
and
J. A. Harrington* and M. Hass
Naval Research Laboratory

1. INTRODUCTION

In the course of studying the spectral emittance of various laser window materials, the alkaline earth fluorides CaF_2, SrF_2, and BaF_2 (grown at Harshaw) and a specially purified crystal of NaF (grown at NRL) were examined. In the present report, these spectra will be presented with emphasis on detection of low-level impurity absorption bands. Multiphonon absorption is reported elsewhere.[1] The actual absorption coefficient at desired laser window wavelengths is not reported here as this is probably limited by current instrumental sensitivity as well as other factors such as scattering. The high-sensitivity apparatus described elsewhere in this report should be capable of at least an order of magnitude higher sensitivity as well as avoiding some of the zero correction problems which occur in the present apparatus.

2. EXPERIMENTAL

The spectral emittance data were obtained using the NELC spectral emittance apparatus. The sample temperature was 100^0C for all crystals.

A. Sodium Fluoride

The spectral emittance of two sodium fluoride crystals grown at NRL by P. H. Klein are shown in Fig. 1.[2] The main spectral feature is the de-

---

* Presently at University of Alabama, Huntsville, Ala.

crease in absorption coefficient as shorter wavelengths are reached. This is associated with intrinsic multiphonon absorption. At short wavelengths, the emittance approaches a constant value [Note change in emittance scale from FS (full scale) at long wavelengths to 0.01 FS (0.01 full scale) at shorter wavelengths in the 3-5 um region]. The origin of this flat or nearly flat region cannot be established as it is comparable in magnitude to the emittance level of an empty sample holder.

A major point to note is that these two crystals differ primarily in the appearance or absence of an absorption band near 6 um. The origin of this impurity absorption is not known and it appears to be a general feature of fluoride crystals examined both in this laboratory and elsewhere. A question which arises in connection with laser windows is whether this band contributes to the absorption at the CO laser window wavelength of 5.3 um and at the DF window wavelength of 3.8 um. It is within the realm of possibility that the wings of this impurity band are sufficiently strong so that it will be detrimental to CO windows, but not to DF windows.

Finally, it should be noted that the vacuum ultraviolet spectra of various crystals of NaF show a well separated impurity band at 151 nm which is associated with OH ions.[2] A corresponding absorption in the 2.7 um region is expected in the infrared. This would be on the verge of detectability using present emittance apparatus and has not been looked for. It is not yet known whether there is a connection between the intensity of the 151 nm band and the 6 um impurity band in the infrared.

B. Calcium Fluoride

The spectral emittance of calcium fluoride in the polycrystalline material

(Harshaw Polytran™) is shown in Fig. 2. No obvious impurity bands are evident in this sample.

The vacuum ultraviolet spectrum has not been studied, but impurity bands (associated with OH) would probably be found.

C. Strontium Fluoride

The spectral emittance of strontium fluoride in the form of polycrystalline material (Harshaw Polytran™) is shown in Fig. 3. Here there appears to be a slight impurity band near 6 um. Since the multiphonon absorption occurs at longer wavelengths in SrF_2, this band would be easier to observe and would be missed if it were of comparable strength in CaF_2. However, it is possible that this band could contribute to absorption at 5.3 um.

D. Barium Fluoride

The spectral emittance of polycrystalline BaF_2 (Harshaw Polytran™) is shown in Fig. 4, while that of single crystal material is shown in Fig. 5. In the case of polycrystalline BaF_2, impurity bands near 6 um and 8 um appear. For the single crystal material, only a band near 6 um is evident. Here again it should be noted that this band is more clearly revealed than in CaF_2 or SrF_2 since the multiphonon absorption is shifted to longer wavelengths. It should also be pointed out that the resolution of the instrument is comparable to the width of the band as indicated in Fig. 4.

3. DISCUSSION AND CONCLUSION.

A study of the fluoride materials NaF, CaF_2, SrF_2, and BaF_2 reveals the presence of an absorption band near 6 um in some materials. The origin of this band has not yet been identified, nor is it known whether this is a

surface absorption band. It is also not clear whether this should be attributed to impurities directly or impurity-induced multiphonon absorption. It should also be pointed out that even in the two- and three- multiphonon region, some structure is evident whose origin is not known.

When this data was first obtained, it was thought that at shorter wavelengths, the deduced absorption coefficients were instrument-limited. However, recent calorimetric measurements by Harrington[1] indicate absorption coefficients (combined surface plus bulk) which are not greatly different (at least by an order of magnitude) from those measured by emittance. For the three polytran samples, the thickness was very nearly 1 cm, so the absorption coefficient equals the emittance (minus the empty sample holder correction) within the accuracy of the measurement.

A number of these questions might be settled by use of refined laser calorimetric measurements and by high sensitivity emittance investigations. It is hoped that studies of this nature can be carried out within the next year.

REFERENCES

1. J. A. Harrington, B.Bendow, S.S. Mitra, K.V. Namjoshi, and D. L. Stierwalt, Appl. Phys. Letters (to be published) and Proc. Fourth Laser Window Conference
2. P. H. Klein, M. Krufeld, and E. W. Claffy, Semiannual ARPA Report No. 4, Naval Research Laboratory, June 30, 1974; P. H. Klein and J. W. Davisson, Proc. Fourth Laser Window Conference
3. M. Hass, J. W. Davisson, H. B. Rosenstock, and J. Babiskin, Proc. Fourth Laser Window Conference

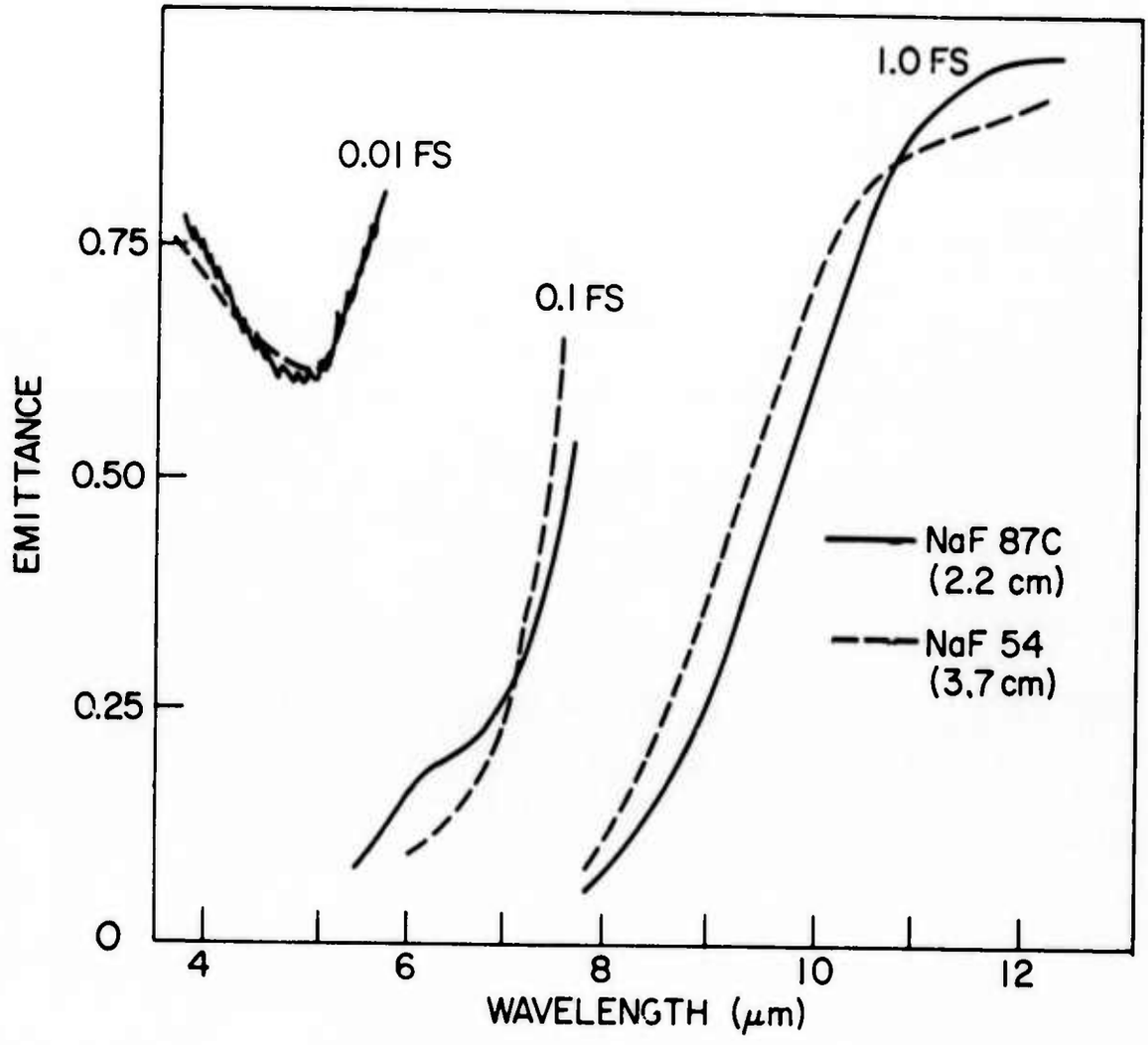

Fig. 1. Spectral emittance of two crystals of NaF. Full scale, 0.1 of FS (full scale)and 0.01 of FS recorder tracings are shown. Note appearance of an impurity band near 6 um.

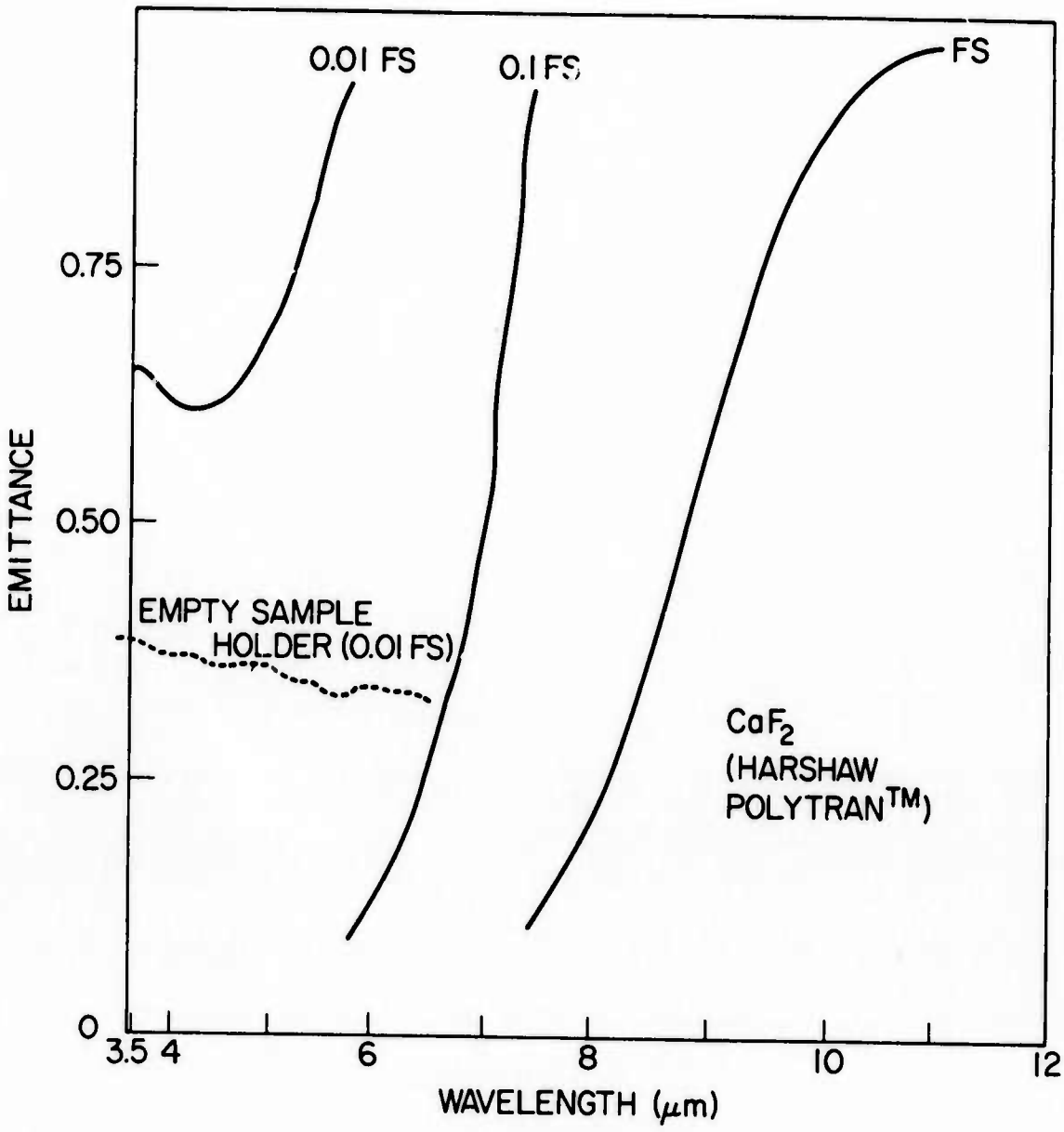

Fig. 2. Spectral emittance of polycrystalline CaF_2. The spectral emittance of an empty sample holder is also shown. No impurity bands are evident.

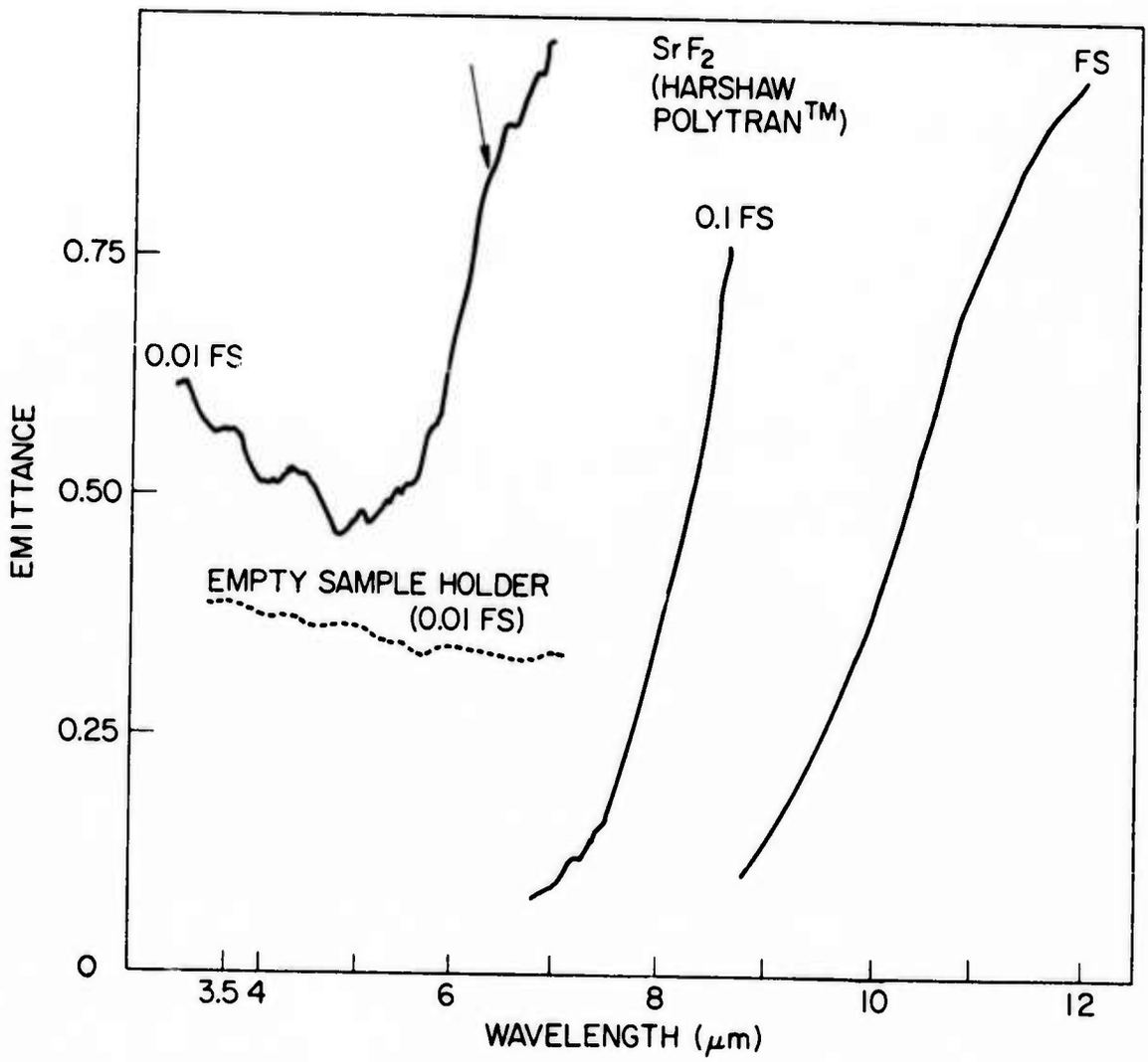

Fig. 3. Spectral emittance of polycrystalline SrF_2. An impurity shoulder near 6 um can be observed as indicated by the arrow.

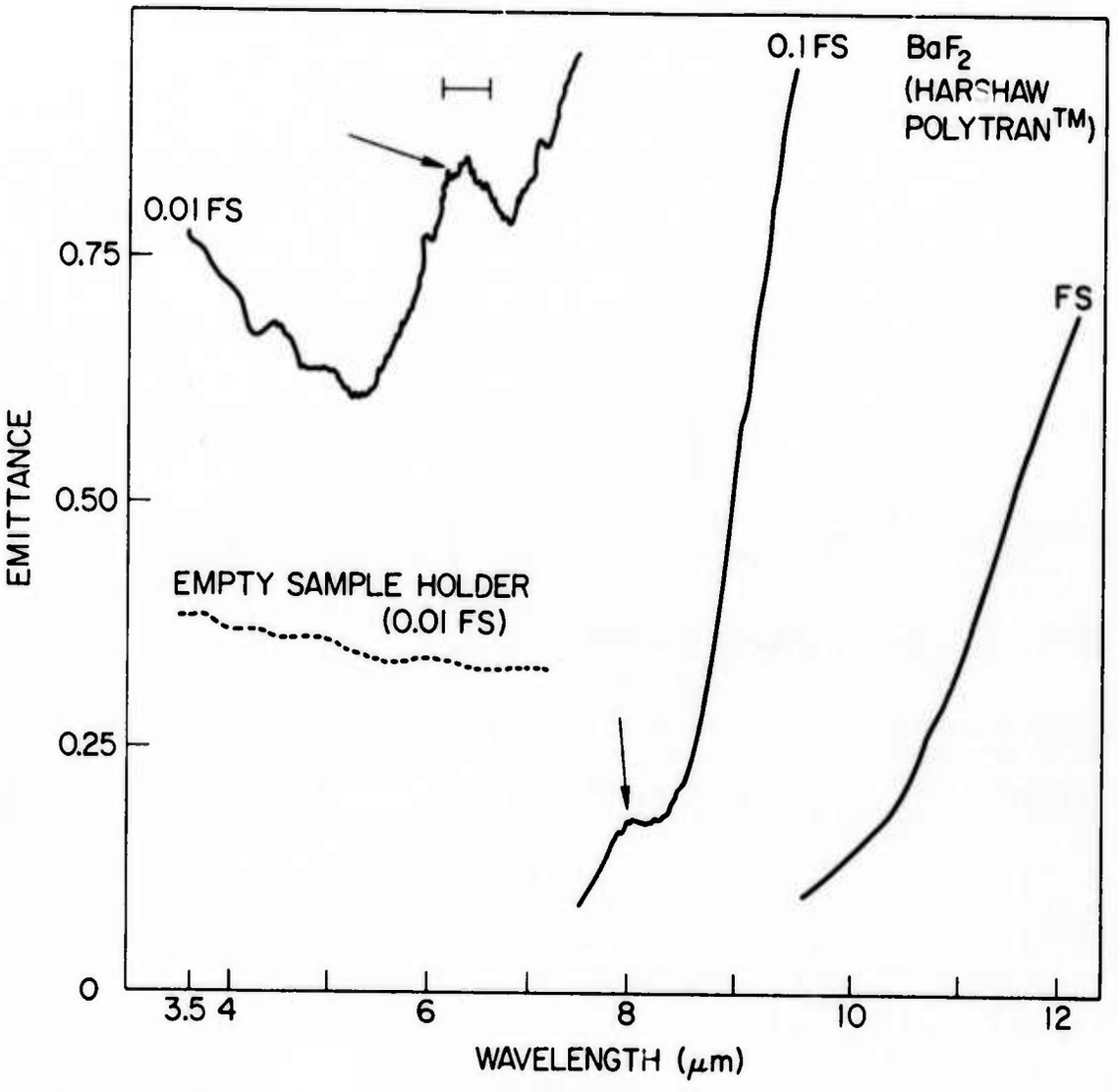

Fig. 4. Spectral emittance of polycrystalline BaF_2. Impurity bands near 6 um and 8 um can be observed as shown by the arrows.

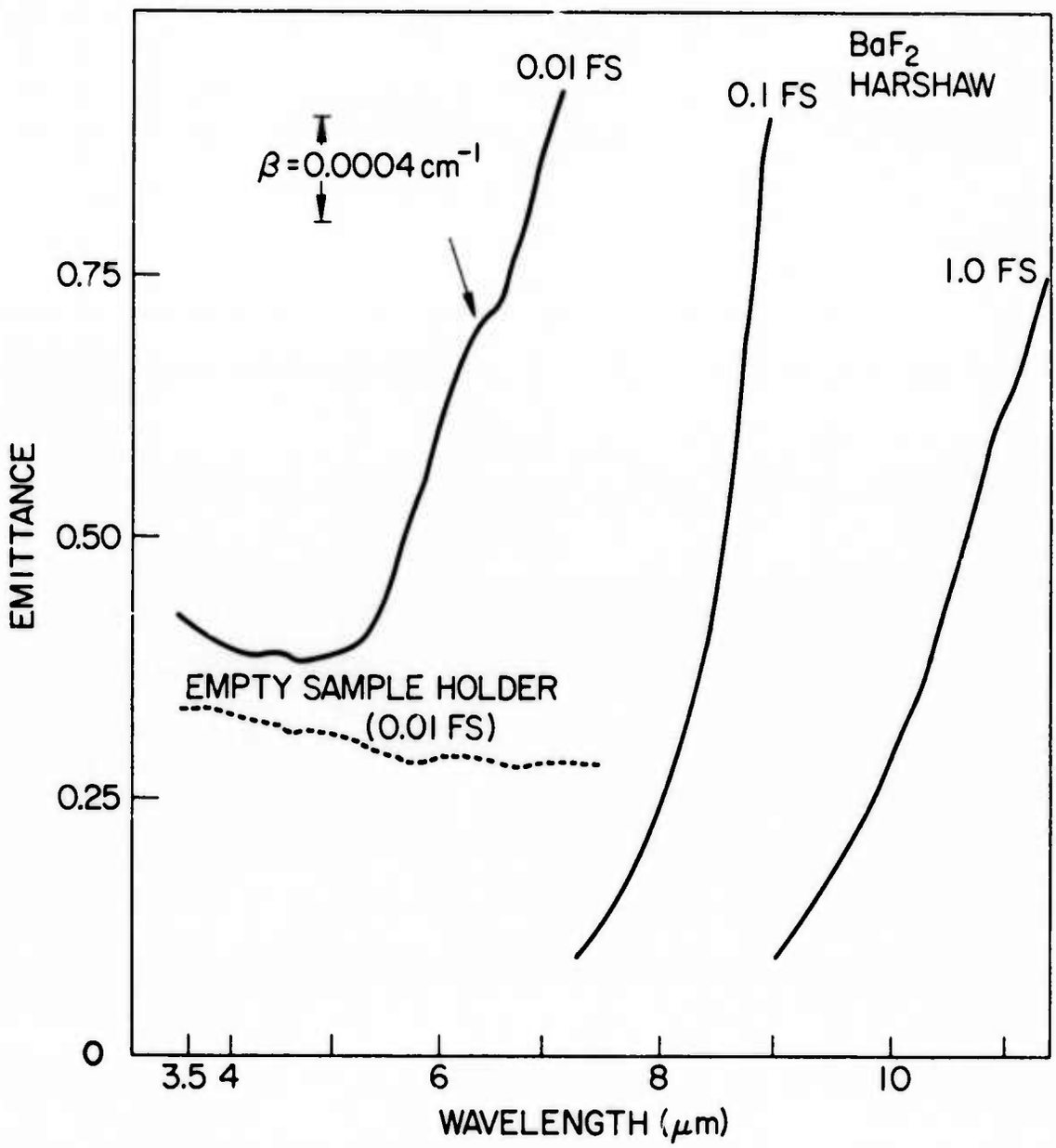

Fig. 5. Spectral emittance of single crystal BaF_2. An absorption band near 6 um is shown by the arrow.

NEW INSTRUMENTATION

Donald L. Stierwalt
Naval Electronics Laboratory Center
San Diego, California

Construction of the high sensitivity cooled wall spectrometer has been largely completed. Current work has been concerned with assembly and testing.

Before painting the inside of the instrument some photographs were taken so the components can be seen more clearly. The vacuum low temperature chamber and the instrument are seen in Fig. 1. In Fig. 2, the moveable filter wheel is indicated. The detector dewar and sample holder are not shown.

A number of problems can be anticipated in achieving high sensitivity. Some of these are instrumental in nature and others are associated with sample preparation. By virtue of experience with existing emittance equipment it is believed that the instrumental problems can be solved. The sample preparation problems are more difficult, but here much insight towards solution of these problems can be obtained from background using laser calorimetric techniques to achieve high sensitivity.

References

1. M. Hass, J. W. Davisson, H. B. Rosenstock, and J. Babiskin, Proc. Fourth Laser Window Conference.

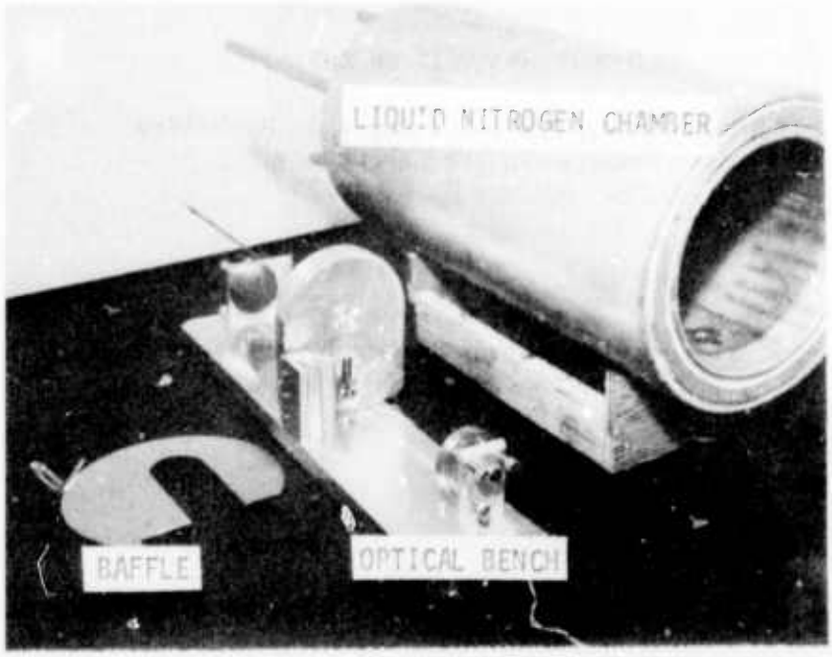

Figure 1. Vacuum Low Temperature Chamber and Instrument.

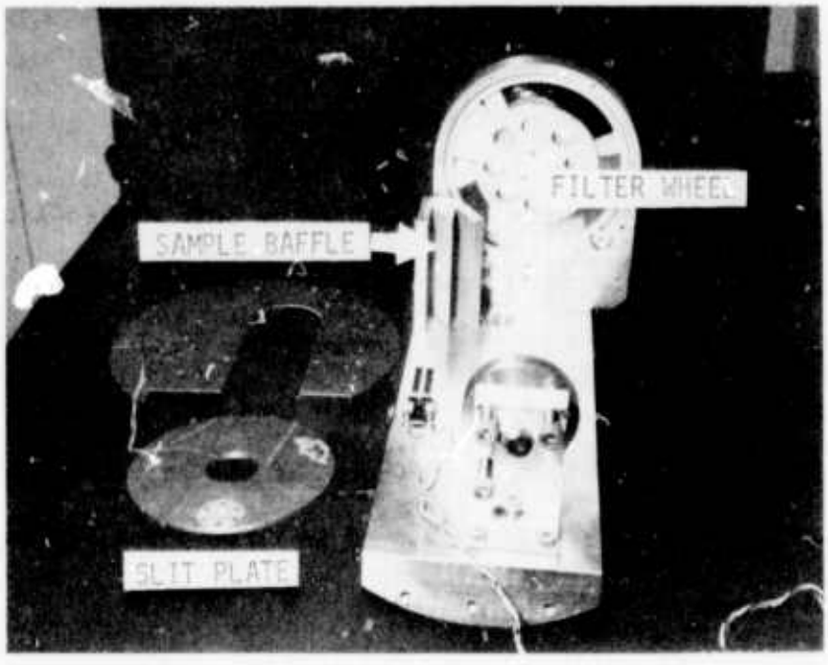

Figure 2. Filter Wheel.

FRACTURE ANALYSIS OF ZnSe*

S.W. Freiman, R.W. Rice and J.J. Mecholsky
Naval Research Laboratory
Washington, D. C. 20375

and

J. C. Wurst**
University of Dayton Research Institute
Dayton, Ohio 45409

1. INTRODUCTION

In the latest report, Rice et al.(1974), several aspects of crack growth and fracture in ZnSe and As_2S_3 laser window materials was discussed. Work has continued on ZnSe in particular and experimental results of slow crack growth and fracture are reported herein as well as the effects on predictions of failure times and proof stresses depending on the source of failure.

2. EXPERIMENTAL PROCEDURE

Crack velocities in CVD ZnSe were measured in both air (50% r.h.) and H_2O using the modified double-cantilever-beam technique of Freiman et al. (1973). A constant load was placed on a specimen ($\approx$ 2" x0.38"x.08") through the use of a weighted pan; crack growth at each load (K_I) was measured with a traveling microscope. The flexural strengths of the halves of the double-cantilever-beam specimens were then measured in three-point bending in both air (50% r.h.) and H_2O.

---

* This work was not done under an ARPA contract but is reported here for the convenience of those concerned with laser windows.

** Work performed under AFML contract No. F33615-72-C-1257

Fracture origins and characteristic fracture features were determined as described by Rice (1973). Since fracture mirrors were generally unclear because of the large ZnSe grain size, the distance from the origin to the onset of macroscopic crack branching was measured along the tensile surface similar to the measurement in glasses, described by Mecholsky, et al. (1974). From this data, the fracture stress can be determined on samples which have fractured in service if the source of failure and branching points can be determined.

3. RESULTS AND DISCUSSION

A. Fracture Analysis

The results of flexural tests of CVD ZnSe specimens (Tables I and II) show that water decreases the strength of ZnSe by approximately 25%. As will be shown later, this reduction is caused by a decrease in the crack propagation resistance of ZnSe due to stress corrosion in water. Flaw sizes in the above specimens calculated using the relationship given in Table I are significantly larger than those observed at the site of fracture initiation. Some differences due to variations in Y(a/b ratio) occur but these are small compared to the differences between calculated and observed flaw sizes. This discrepancy is due to the use of the polycrystalline fracture energy (3.4 J/m^2) in the calculations rather than the single crystal value, as would be correct for these cases where the flaw size is smaller than the grain size, as suggested by Rice (1974) and Freiman, et al. (1974).

Strength as a function of grain size (or flaw size) at the fracture origin is shown in Fig. 1. Strengths are plotted as a function of the size of the specific grain observed at the origin of fracture except in a few

cases where two very closely aligned grains at the origin were treated as one grain or larger grains were clearly observed to have had flaws smaller than the grain size. In these few cases the two grains and the actual flaw size respectively were used. Previous data of Wurst (1973) showing strength versus average grain size of various ZnSe is shown for comparison. If it is assumed that this grain size is about the flaw size (except in the few cases where other flaw sizes are noted), then the slope of the strength-grain size curve gives a fracture energy of ~ 1 J/m^2, in good agreement with the estimate (Semiannual Report No. 4, June 1974). The fact that the flaw size in the one case where the large grain at the origin clearly had a flaw smaller than the grain falls on the curve of Fig. 1 lends strong support to the idea of fracture energies being close to those of single crystals.

The fracture stress of ZnSe is plotted in Figure 2 as a function of the distance from the origin of failure to macroscopic crack branching. The slope of the line is drawn as -0.5 because it is assumed that the relationship, $\sigma \sqrt{r}$ = constant, is valid for this material as found in other ceramics. Although this relationship is usually shown for inner and outer mirror radii, it is equally valid for crack branching and in fact, for this material which has large grain sizes (20-300μm), crack branching is much more easily measured than either the radii usually attributed to mist and hackle. This relationship is useful because it can enable the observer to determine the failure stress by locating the approximate source of failure from the crack pattern and measuring the distance to the point of macroscopic crack branching. Thus, in-service failures may be examined and analyzed, if necessary, to determine their cause.

B. Crack Propagation

As shown in Figure 3, slow crack growth occurs in ZnSe. The fact that the presence of water at the crack tip plays a significant role in this process is demonstrated by the increased crack velocity at a given K_I when the ZnSe was tested in water. This effect of water on crack propagation is also reflected in the decreased flexural strength of ZnSe under the same conditions (Tables I and II). The scatter in the slow crack growth data for ZnSe is attributed to its large grain size (up to 300μ). In theory, one could use this K-V data to predict times to failure for ZnSe under stress as suggested by Evans and Wiederhorn (1974). The discrepancy between predicted and observed flaw sizes using polycrystalline fracture mechanics data suggests, however, that care should be taken in using the data in this way since a crack propagating through just one large grain may cause it to reach a critical length at a correspondingly lower K_I.

Although its exact form is not known, it is theorized that the mechanism of stress corrosion in ZnSe is quite similar to that for glasses. Under the influence of the crack tip stress, which adds elastic energy to the bonds, H_2O can react with ZnSe according to:

$$ZnSe + 2H_2O \rightarrow Zn(OH)_2 + H_2Se \qquad (1)$$

This reaction would weaken the bonding in the ZnSe and allow cracks to extend. Whether the reaction of OH^- or H^+ is the rate controlling step in the process is not known.

C. Failure Predictions

The fact that failure in ZnSe usually takes place from flaws smaller than the grains and is governed by a fracture energy of 1 J/m^2 rather than

the higher polycrystalline value has important implications in the use of fracture mechanics, proof testing, and nondestructive evaluation to assure safe lifetimes of laser windows. While Evans and Johnson (1974) noted this possibility, they performed no analysis. Based on the fact that crack velocities in ZnSe can be empirically expressed as a function of stress intensity, K_I, by:

$$V = AK_I^n \tag{2}$$

The minimum time to failure at an applied stress, σ_a is given by (Wiederhorn (1974)).

$$t_{min} = \frac{2\,\sigma_a^{-2}\,K_{IC}^{2-n_P}\,n-2}{AY^2\,(n-2)} \tag{3}$$

where P is the proof test ratio, $\sigma p/\sigma a$

Y is a constant based on flaw geometry

K_{IC} is the stress intensity necessary to produce rapid fracture.

Using Eq. 3, a calculation was made of the effect of failure within a single grain on the time to failure. It was assumed that the slope of the V-K curve, n, for single crystal ZnSe is the same as the polycrystalline value, i.e. ~40. K_{IC} for the single crystal was taken as .37 $MN/m^{3/2}$ (γ_c=1 J/m^2) while that for polycrystalline material was taken as .90 $MN/m^{3/2}$ (γ_c=5.6 J/m^2). The latter value corresponds to a crack velocity of 10^{-1} m/sec and is the same value used by Evans and Johnson (1974). The fact that the measured value of γ_c is smaller than .9 $MN/m^{3/2}$ suggests that the large grains may cause a reduction in γ_c. For a given σ_a and proof test ratio, t_{min} varies as $\frac{K_{IC}^{2-n}}{A}$. From the values of this parameter shown in Table 3, one can see that failure in ZnSe would occur 20 times sooner than predicted from strictly polycrystalline data. This could be somewhat misleading, however,

since normally a lifetime for a structure is chosen, and a proof test ratio calculated to assure no failures within that time. Performing these calculations, one obtains that to assure the same lifetimes, the actual proof test ratio should be ≈1.1 times that calculated using polycrystalline data. This means that the proof test ratio should be ≈1.4 - 1.45 rather than 1.3 - 1.35 as suggested by Evans and Johnson (1974), where proof tests are conducted in an environment in which no slow crack growth will occur while the proof load is being removed. Use of this higher ratio would mean the loss of more windows during proofing but is the most conservative in terms of assuring no window losses during service.

The fact that failure in ZnSe essentially takes place within one grain also means that critical flaw sizes are of the order of 50-100μ (Table 1) rather than millimeters as suggested by Evans and Johnson. Flaws of 50-100μ would be predicted using 1 J/m^2 as γ_c. These smaller flaw sizes greatly reduce the likelyhood of detection by any current NDE technique, so that a proof testing will undoubtedly be necessary.

4. SUMMARY

It has been shown that H_2O causes stress-corrosion in ZnSe allowing cracks to grow under loads below those which produce fast fracture. It was also indicated that cracks within individual grains can grow at even lower stresses. This work suggests that ZnSe windows must be designed with slow crack growth processes in mind. Hermetic seals are uncertain since anti-reflection coatings, even if impervious to H_2O (including the edges) must be insensitive to stress-corrosion. Recent NRL studies indicate MgF_2 and As_2S_3 to be susceptible to stress corrosion, suggesting that other

related coating materials may also be. Questions regarding the H_2O permeability and stress corrosion sensitivity of anti-reflection coatings remain to be answered.

REFERENCES

1. A.G. Evans and S.M. Wiederhorn (1974), J. Mat. Sci., 9: 270.
2. A.G. Evans and H. Johnson (1974), Submitted to J. Am. Ceram. Soc.
3. S.W. Freiman, D.R. Mulville, and P.W. Mast (1973), J. Mat. Sci. 8. 1527.
4. S.W. Freiman, K.R. McKinney, and H.L. Smith (1974), pp. 659-676 in Fracture Mechanics of Ceramics, R.C. Bradt, D.P.H. Hasselman and F.F. Lange, eds., Plenum Publishing Corp., New York.
5. J.J. Mecholsky, R.W. Rice, and S.W. Freiman (1974), J.Am. Ceram. Soc. 52: 440.
6. R.W. Rice, (1973) to be published in the Proceedings of the Symposium on Surfaces and Interfaces in Glass and Ceramics, held at Alfred University.
7. R.W. Rice (1974), pp. 323-346, in Fracture Mechanics of Ceramics, R.E. Bradt, D.P.H. Hasselman and F.F. Lange, eds., Plenum Publishing Corp., New York.
8. J.J. Wurst (1973), Quarterly Progress Report Nos. 1-6, Air Force Materials Laboratory, Wright-Patterson Air Force Base, Contr. No. F33615-72-C-1257.

TABLE I

Fracture Strength and Flaw Size in ZnSe Tested in Air

Specimen Designation	Flexural Fracture Strength MN/m^2	Observed Flaw Sizes* μm a	b	Predicted Flaw Size** μm
UDRI 96-2B	24			400
NRL 0802-11	27	40	50	318
NRL 0802-12	27	40	200	318
UDRI 96-3B	29			285
UDRI 60-1	30	15		252
UDRI 5a-2+	33			214
NRL 0802-13	33	110	65	214
UDRI 61-C-24-4	34			208
NRL 0802-9	36			182
NRL 0802-8	36	110	275	182
NRL 0802-10	37	40	55	169
UDRI 61-C-41-1	38	10		158
UDRI 60-2	41	10		138
NRL-0314-5	48	20	35	100
NRL-0314-1	50	20	35	92
NRL-0314-3	50	30	43	92
NRL-0314-2	56	28	50	75
UDRI-82-6	58			69
UDRI-94-8D	58			69
NRL 0314-4	59	50	80	68
Average Strength	40			
95% Confidence Limits	± 5			

+ PVD

* a = flaw depth; b = flaw half-width

** $a = E\gamma Y^2/(\sigma^2)$ where $E = 6.9 \times 10^4$ MN/m^2, $\gamma = 3.4$ J/m^2, σ is the stress in MN/m^2, and Y was chosen to be 1 corresponding to $\frac{a}{b} = 0.8$.

TABLE II

Fracture Strength and Flaw Size in ZnSe Tested in Water

Specimen Designation	Flexural Fracture Strength MN/m^2	Observed Flaw Sizes a	b	Predicted Flaw* Sizes
NRL 0802-2	25	110	30	371
NRL 0802-4	26	30	60	343
NRL 0802-5	27	200	250	318
NRL 0802-6	32	120	225	229
NRL 0802-3	36	30	35	182
Average Strength	29			
95% Confidence Limits	± 5			

*Predicted using polycrystalline fracture energies as in Table I.

TABLE III

	K_{IC} ($MN/m^{3/2}$)	n	A	$\frac{K_{IC}^{(2-n)}}{A}$
Single Crystal	0.37	40	1.9×10^{16}	1.4
Polycrystal	0.90	40	2.0	28

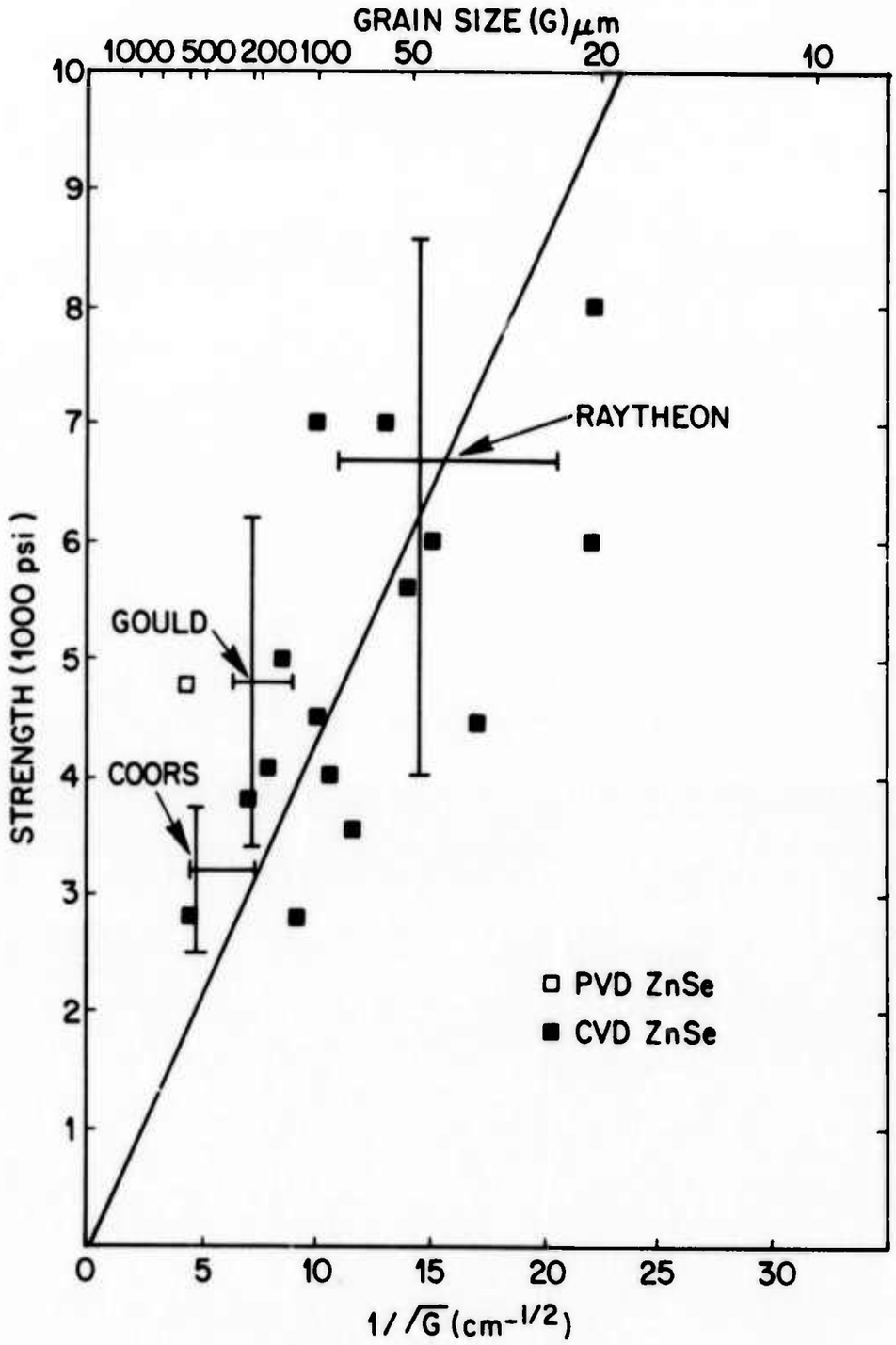

Figure 1. Fracture Strength as a function of the grain size at the fracture origin in ZnSe. Points with error bars are those tested by Wurst (1973).

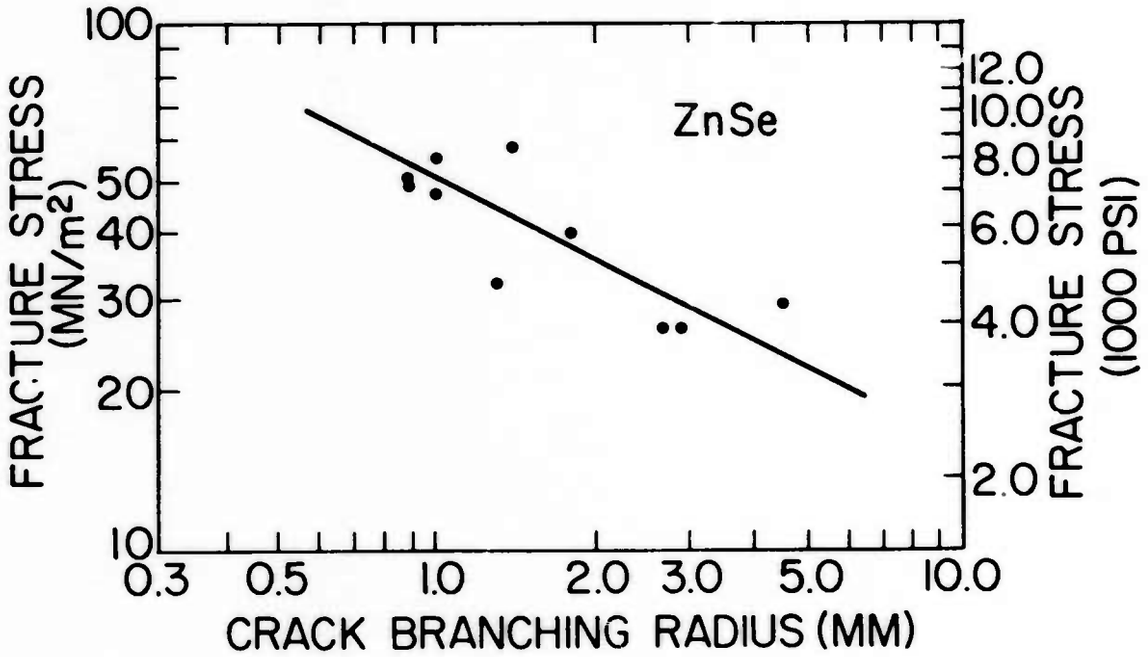

Figure 2. Fracture strength as function of the distance to the point of crack branching in ZnSe, where this distance was measured along the tensile surface.

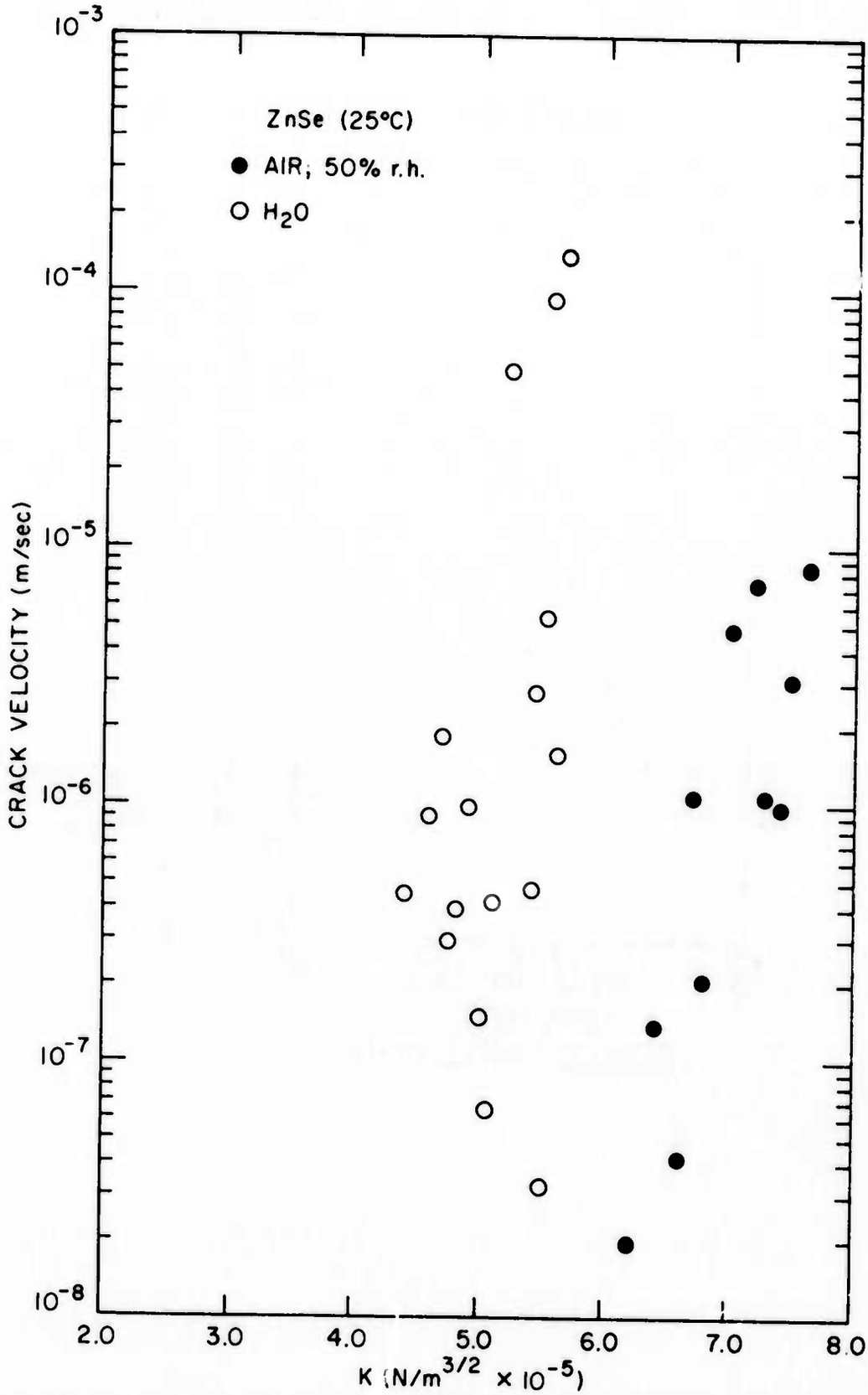

Figure 3. Crack velocity as a function of stress intensity factor, K, in ZnSe.